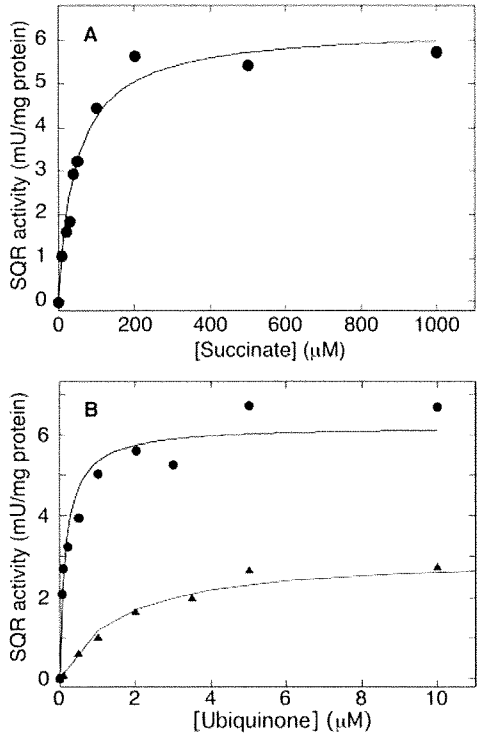


Fig. 1. **Kinetic analysis of SQR activity of *P. y. yoelii* mitochondria.** (A) As a function of the succinate concentration, SQR activity was examined at 6 μg mitochondrial protein/ml in the presence of 0.1 mM $Q_2$. Data points were averages from three independent preparations (6.19 ± 0.93 mU/mg protein with 1 mM succinate and 0.1 mM $Q_2$). Data were fitted to Michaelis–Menten kinetics with apparent $K_m$ and $V_{max}$ values of 49.3 ± 7.0 μM and 6.26 ± 0.27 mU/mg protein, respectively. (B) As a function of the $Q_1$ (circles) or $Q_2$ (triangles) concentration, SQR activity was examined in the presence of 10 mM succinate. Data points were averages from two independent preparations (6.25 ± 0.87 mU/mg protein with 1 mM succinate and 0.1 mM $Q_2$). Data were fitted to Michaelis–Menten kinetics with apparent $K_m$ and $V_{max}$ values of 1.61 ± 0.20 μM and 3.03 ± 0.12 mU/mg protein, respectively, for $Q_1$ and 0.17 ± 0.04 μM and 6.20 ± 0.30 mU/mg protein, respectively, for $Q_2$.

*Membrane Anchor Subunits of Plasmodium Complex II*—For reduction of ubiquinone, *Plasmodium* complex II should have a quinone-binding pocket provided by Ip and the CybL/CybS heterodimer (*30–32*). For the examination of subunit structure of *Plasmodium* complex II, we first determined the molecular weight of *P. y. yoelii* complex II by hrCNE, followed by in-gel activity staining as phenazine methosulphate-mediated succinate : NBT reductase. An apparent molecular weight of *P. y. yoelii* complex II was estimated to be 135 kDa (Fig. 3, lane 2), which is comparable to 130 kDa of bovine and yeast complex II (*33*). Western blot analysis identified Fp and Ip as the 70- and 35-kDa proteins, respectively (Fig. 3, lanes 3 and 4), indicating that a sum of molecular weights of membrane anchor subunits is about 30 kDa. Subsequently, the 135-kDa bands in hrCNE were excised from gels and subjected to SDS–PAGE analysis. Due to an extremely low activity of *Plasmodium* complex II (~1% of mammalian mitochondria) and the diffusion of

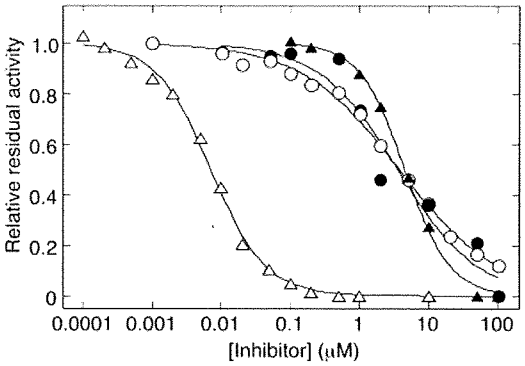


Fig. 2. **Inhibition of SQR activity of *P. y. yoelii* mitochondria by atpenin A5 and carboxin.** SQR activity of *P. y. yoelii* (closed symbols) and rat liver (open symbols) mitochondria was determined with 10 mM potassium succinate and 0.1 mM $Q_2$ in the presence of atpenin A5 (triangles), and carboxin (circles). Data points were average values from two independent preparations. $IC_{50}$ values were determined to be 4.6 ± 0.2 μM for atpenin A5 and 3.6 ± 1.0 μM for carboxin in *P. y. yoelii* mitochondria and 7.1 ± 0.3 nM for atpenin A5 and 3.8 ± 0.1 μM for carboxin in rat liver mitochondria. Control activitiy of *P. y. yoelii* mitochondria was 2.68 ± 0.03 mU/mg protein.

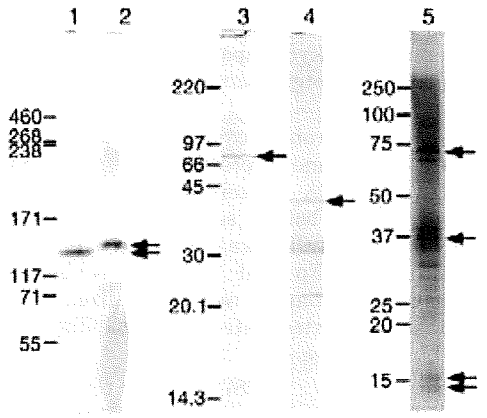


Fig. 3. **Electrophoresis analysis of complex II in *P. y. yoelii* mitochondria.** Solubilized mitochondrial proteins were subjected to hrCNE, and complex II of bovine (lane 1, 2.4 μg protein) and *P. y. yoelii* (lane 2, ~0.4 mg protein) mitochondria were visualized by SDH activity staining. Arrows indicate complex II bands. For Western blot analysis, 10 μg of mitochondrial proteins were subjected to 15% SDS–PAGE and Fp (lane 3) and Ip (lane 4), indicated by arrows, were identified by anti-PfFp and anti-PfIp rabbit antisera, respectively. For identification of *P. y. yoelii* complex II subunits, complex II bands in hrCNE were excised from gels and subjected to 10–20% SDS–PAGE, followed by silver staining (lane 5). Putative subunits of *P. y. yoelii* complex II are indicated by arrows. HiMark Prestained High Molecular Weight Protein Standard (Invitrogen), Rainbow Colored Protein Molecular Weight Marker (High molecular weight range) (Amersham Pharmacia Biotech), and Precision Plus Protein Standard (Bio-Rad) were used as molecular weight standards for lanes 1 and 2, lanes 3 and 4, and lane 5, respectively.

a reduced product of NBT, it was difficult to cut out the complex II band but we were able to identify 70, 35, 16 and 14 kDa bands as putative subunits of the 135-kDa complex (Fig. 3, lane 5).

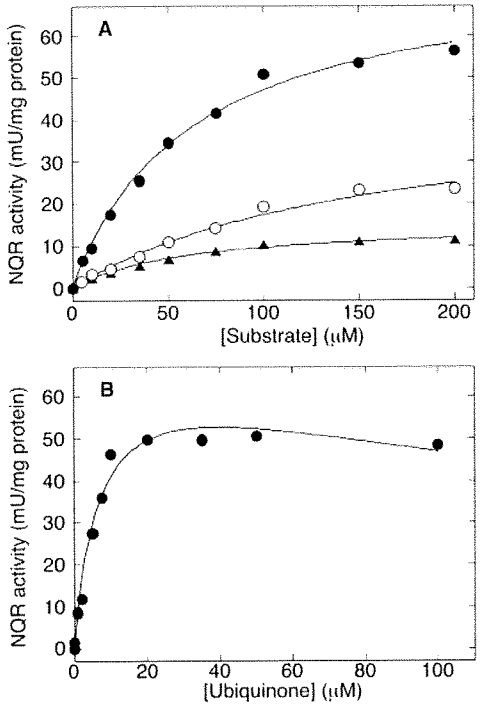


Fig. 4. **Kinetic analysis of NQR activity in *P. y. yoelii* mitochondria.** (A) As a function of the concentration of NADH (closed circle), NADPH (open circle) or deamino-NADH (closed triangle), NQR activity was examined at 6 μg protein/ml in the presence of 0.1 mM $Q_1$. Data points were averages from two independent preparations (44.9 ± 4.8 mU/mg protein with 0.2 mM NADH). Data were fitted to Michaelis–Menten kinetics with apparent $K_m$ and $V_{max}$ values of 63.2 ± 6.9 μM and 76.7 ± 3.4 mU/mg protein, respectively, for NADH, 157 ± 33 μM and 44.4 ± 5.4 mU/mg protein, respectively, for NADPH, 58.4 ± 5.7 μM and 15.1 ± 0.6 mU/mg protein, respectively, for deamino-NADH. (B) As a function of the concentration of $Q_1$, NQR activity was examined in the presence of 0.2 mM NADH. Data points were average values from two independent preparations [48.6 ± 7.9 mU/mg protein at 0.1 mM $Q_1$). Data were fitted to substrate inhibition kinetics with apparent $K_m$, $V_{max}$ and $K_{is}$ values of 7.2 ± 1.7 μM, 71.8 ± 7.6 mU/mg protein, and 218 ± 97 μM, respectively, using the equation $v = V_{max}\ S/(K_m + S + S\ (1+S/K_{is}))$.

*Enzymatic Properties of Plasmodium NDH-II*—*Plasmodium* spp. lacks genes encoding complex I (*6*, *7*) and uses a single-subunit NADH dehydrogenase (NDH-II) (*8*, *15*). Upon permealization of mitochondria with 30 μg/ml alamethicin, which forms pores large enough to permit the rapid diffusion of NADH (*34*), NQR and SQR activities increased 32% and 27%, respectively, indicating that *Plasmodium* NDH-II is likely located at the matrix side of the inner membrane.

When reactions were started by addition of NADH, NQR activity showed a simple Michaelis–Menten kinetics with apparent $K_m$ and $V_{max}$ values of 63 μM for NADH and 77 mU/mg protein, respectively (Fig. 4A). $K_m$ value for NADH was closer to 31 μM of *Saccharomyces cerevisiae* internal NDH-II (NDI1) (*35*) and 34 μM of *E. coli* NDH-II (*36*) than 15 μM of yeast *Yarrowia lipolytica* external NDH-II (NDE) (*37*). In contrast,

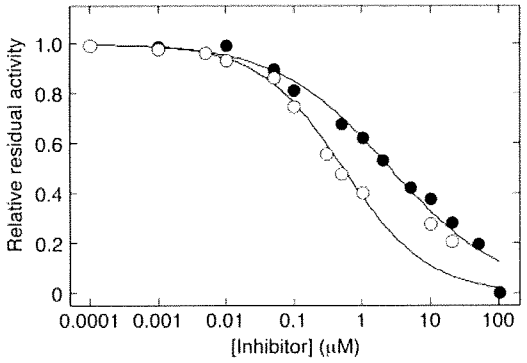


Fig. 5. **Inhibition of NQR activity of *P. y. yoelii* mitochondria by HQNO and Aurachin C1-10.** NQR activity of *P. y. yoelii* mitochondria was determined with 0.2 mM NADH and 0.1 mM $Q_1$ in the presence of HQNO (closed circle) or aurachin C1-10 (open circle). Data points were average values from two independent preparations. Control activity of *P. y. yoelii* mitochondria was 45.6 ± 1.3 mU/mg protein with 0.1 mM $Q_1$. $IC_{50}$ values for HQNO and aurachin C1-10 were estimated to be 2.5 ± 0.4 and 0.47 ± 0.03 μM, respectively.

$Q_1$-started NQR activity showed substrate inhibition kinetics with $K_m$ and $K_{is}$ values of 7 and 218 μM, respectively, for $Q_1$ (Fig. 4B). Unlike *E. coli* NADH-II (*36*) and *Y. lipolytica* NDE (*37*), *P. y. yoelii* NDH-II can oxidize deamino-NADH ($K_m$ = 58 μM, $V_{max}$ = 15 U/mg protein) and NADPH ($K_m$ = 157 μM, $V_{max}$ = 44 mU/mg protein) (Fig. 5A). $V_{max}/K_m$ ratios indicate that *Plasmodium* NDH-II is more specific to NADH compared to NAD(P)H dehydrogenases from red beet root mitochondria [NDI (*38*) and NDE (*39*)].

Since mammalian hosts lack NDH-II, this enzyme is a promising target for new antiplasmodial agents. However, inhibitors for NDH-II are rare and mostly unspecific (*34*). Fry *et al.* (*11*) examined effects of inhibitors on ATP level in erythrocytic *P. falciparum* and found that 2-heptyl-4-hydroxyquinoline *N*-oxide (HQNO) and 5-hydroxy-2-methyl-1,4-naphthoquinone (plumbagin) showed antimalarial activities with $IC_{50}$ values of 4.0 and 3.5 μM, respectively. In yeast, quinolone analogues HQNO and aurachin C 0-11 were shown to inhibit NDI1 with the $IC_{50}$ values of 8 and 0.2 μM, respectively (*40*). In this study, we examined effects of HQNO and aurachin C 1-10 (*41*) on NADH:$Q_1$ reductase activity and determined $IC_{50}$ values to be 2.5 and 0.5 μM, respectively (Fig. 5). Our data indicate that the quinolone analogues are potent inhibitors for *Plasmodium* NDH-II. Trifluoroperazine, the uncompetitive inhibitor in terms of $Q_2$ for *Mycobacterium tuberculosis* NDH-II ($IC_{50}$ = 12 μM) (*42*), reduced the NADH:$Q_1$ reductase activity to 26% of the control at 100 μM.

## DISCUSSION

*Properties of Plasmodium Complex II*—Parasitic nematodes adapted to hypoxic host environments, have modified respiratory chain, where isoforms of complex II serve as fumarate reductase (*43*, *44*). Kinetic properties of *P. y. yoelii* complex II are similar to those of mammalian enzymes and thus suitable for catalysing the

Table 2. **Effects of quinone-binding site inhibitors on SQR activity of *P. y. yoelii* mitochondria.**

| 100 μM inhibitor | *P. y. yoelii* mitochondria | Rat liver mitochondria |
|---|---|---|
| Control | 100% | 100% |
| Atpenin A5 | <0.4 | <0.05 |
| Carboxin | <0.4 | <0.05 |
| Flutoranil | 58 | 22 |
| TTFA | 80 | 12 |
| HQNO | 54 | 94 |
| Plumbagin | 52 | 98 |
| DNP-17 | 67 | 99 |

Control activities (mean ± SD) were 2.66 ± 0.02 (*P. y. yoelii*) and 180 ± 5 (rat liver) mU/mg protein.

forward reaction of TCA cycle (i.e. the oxidation of succinate). It should be noted that *Plasmodium* complex II was more resistant to known quinone-binding site inhibitors for mammalian complex II (Table 2), probably due to the divergence of membrane anchor subunits of *Plasmodium* complex II.

From the whole cell lysate of *P. falciparum*, Suraveratum *et al.* (*28*) purified complex II as the Fp/Ip heterodimer with an apparent molecular weight of 90 kDa and claimed that it has a much lower $K_m$ value (3 μM) for succinate and plumbagin-sensitive SQR activity. However, the concentration (0.2%) of octyl glucoside used for the isolation of *P. falciparum* complex II was not enough for the solubilization of membrane proteins (i.e. critical micell concentration of octyl glucoside is 0.73%). Octyl glucoside likely dissociates the Fp/Ip dimer from the membrane anchor and the aerobic isolation of the Fp/Ip dimer would damage the iron–sulphur clusters in Ip. Thus, SQR activity of such preparations need to be carefully examined.

*Plasmodium* CybL and CybS are still not annotated in the current database (*6*, *7*), likely due to the divergence from ortholog sequences. However, 2D–PAGE analysis (Fig. 3), SQR activity (Fig. 1, refs. *20*, *25*) and the structure of quinone-binding site in complex II (*30–32*) support the presence of these membrane anchor subunits in *Plasmodium* spp. In membrane anchors of complex II, "$Rx_{16}Sx_2HR$" (helix I) and '$YHx_{10}D$' (helix II) motifs in CybL and '$LHx_{10}DY$' (helix II) motif in CybS are conserved for quinone/haem binding. And only such motifs are conserved in protist membrane anchors (*45*). One candidates for *P. y. yoelii* CybL (accession no. XP_731082, 10,086 Da) and one candidate for CybS (accession no. XP_726783, 10,379 Da) can be identified from 3,310 ORFs shared by *P. falciparum* and *P. y. yoelii* on the basis of the size (<200 amino acid residues), the presence of transmembrane segments (≤3), and the quinone/haem-binding motifs. PyCybL and PyCybS have two transmembrane regions and contain the quinone/haem-binding motifs, '$Rx_{14}Sx_2HY$' and '$YYx_{10}DY$' motifs and '$Yx_{10}G$' motif, respectively. In *S. cerevisiae* strain S288C (Baker's yeast), CybS (accession no. NP_010463) uses the $Yx_{10}DY$ motif, and the His-to-Tyr mutant of the CybL $YHx_{10}D$ motif retained a half of the enzyme activity and haem (*46*). Thus, in *Plasmodium* CybL and CybS, Tyr could also substitute the role of the conserved His residue in membrane anchor subunits. Although it has to be tested by protein chemically in future studies, our data support that the subunit structure of *Plasmodium* complex II is similar to that of mammalian complex II.

*Properties of Plasmodium NDH-II*—Previously, Krungkrai *et al.* (*47*) isolated mitochondrial complex I from *P. falciparum* and *P. berghei* as a 130-kDa complex containing 38- and 33-kDa subunits. They claimed that NADH:ubiquinone-8 reductase activity was sensitive to rotenone ($IC_{50}$ = 12 μM) and plumbagin ($IC_{50}$ = 6 μM). However, NDH-I is not encoded by the *Plasmodium* genomes (*6*, *7*) and concentrations of *n*-octyl glucoside used for the solubilization and purification were below its critical micelle concentration (CMC) where *n*-octyl glucoside cannot serve as a detergent. Alternative NADH dehydrogenase NDH-II is a rotenone-insensitive single-subunit enzyme (*15*, *34*) and the apparent molecular weights and subunit structure of *P. falciparum* (acc. no. XP_001352022 and MW 61,670) and *P. y. yoelii* (acc. no. XP_731423, MW 66,156) NDH-II are totally different from those reported by Krungkrai *et al.* (*47*). The $IC_{50}$ value of mouse liver mitochondria for rotenone (8.4 μM; Table 3 in ref. 47) was three orders of magnitude higher than the $IC_{50}$ reported for mammalian enzymes (*26*). Recently, Biagini *et al.* (*15*) used the whole cell lysate of *P. falciparum* and claimed that PfNDH-II was inhibited by diphenylene iodonium chloride (DPI, $IC_{50}$ of 15–25 μM) and diphenyl iodonium chloride (IDP, $IC_{50}$ = 66 μM). As pointed out by Vaidya *et al.* (*48*), the $IC_{50}$ for the enzyme was 100- and 10-fold higher than those for the growth inhibition and other NADH oxidases in the lysate may contribute to the activity. Very recently, it was reported that purified recombinant PfNDH-II was not inhibited by known NDH-I inhibitors and flavoenzyme inhibitors (DPI and IDP) (Dong, C., Patel, V., Clardy, J., and Wirth, D., personal communication). Thus, previous studies on *Plasmodium* NDH-II need to be reexamined. Our data indicate that *Plasmodium* NDH-II is a member of internal NDH-II (Ndi), which reoxidizes NADH in the mitochondrial matrix. Recently, Saleh *et al.* (*49*) demonstrated the antiplasmodial activity ($IC_{50}$ = 14 nM) of 1-hydroxy-2-dodecyl-4(1*H*)quinolone (HDQ), which has been identified as the potent inhibitor for *Y. lipolytica* NDE ($IC_{50}$ = 0.2 μM) (*50*), demonstrating that *Plasmodium* NDH-II is a promising target for new drugs.

*Oxidative Phosphorylation in Plasmodium Mitochondria*—For a long time, it has been assumed that *Plasmodium* mitochondria cannot carry out oxidative phosphorylation (*4*, *5*) because of a lack of membrane anchor subunits of ATP synthase (*9*, *11*). Oxidative phosphorylation, succinate respiration (*8*, *17*), and effects of respiratory complex inhibitors on the generation of membrane potential (*16*) in rodent malaria mitochondria support the notion that *Plasmodium* mitochondria are fully capable of oxidative phosphorylation. Careful analysis of current genome databases (*6*, *7*) with partial subunits sequences of *Crithidia fasciculata* (*51*) and *Leishmania tarentolae* (*52*) could identify ten subunits of *P. falciparum* $F_oF_1$-ATP synthase, including membrane anchor subunits *a* (XP_001347344) and *b* (XP_001348969) (Mogi, T. and Kita, K., unpublished

results), which are found to be highly divergent from eukaryotic and bacterial counterparts. Thus, all canonical subunits of complex II and ATP synthase are present in *Plasmodium* spp., and malaria parasites can yield energy *via* oxidative phosphorylation. The *in vivo* expression profiles of parasites derived from infected patients showed the up-regulation of these enzymes under conditions similar to starvation in yeast (*18*).

## CONCLUSION

We isolated active mitochondria from rodent malaria *P. y. yoelii* from infected mouse erythrocytes and characterized complex II and NDH-II. *Plasmodium* complex II is the four-subunit enzyme but its quinone-reduction site in the membrane anchor subunits seems structurally different from that of mammalian enzyme. *Plasmodium* NDH-II showed enzymatic properties similar to those of NDI and quinolones were found to be potent inhibitors. Alternative respiratory enzymes, which are absent in mammalian mitochondria, are as promising targets for new antibiotics (*53*, *54*). We hope that our findings will help understanding of energy metabolism in malaria parasites and the development of new antimalarial drugs.

## FUNDING

This study was supported in part by a grant-in-aid for scientific research (20570124 to T.M.), scientific research on Priority Areas (18073004 to K.K.) and Creative Scientific Research (18GS0314 to K.K.) from the Japanese Ministry of Education, Science, Culture, Sports, and Technology. We thank Dr H. Ohtsuki (Ehime University) for *P. y. yoelii* strain 17XL, Dr. D. Wirth (Harvard School of Public Health) for the use of unpublished results prior to publication, and Ministry of Health, Labour and Welfare for financial supports.

## CONFLICT OF INTEREST

None declared.

## REFERENCES

1. World Health Organization (2007) Malaria Elimination. A field manual for low and moderate endemic countries. World Health Organization, Geneva, Switzerland
2. Hyde, J.E. (2005) Drug-resistant malaria. *Trends Parasitol.* **21**, 494–498
3. Sherman, I.W. (1998) Carbohydrate metabolism of asexual stages. in *Malaria, Parasite Biology, Pathogenesis and Protection* (Sherman, I.W., ed.), pp. 135–143, ASM Press, Washington, DC
4. Vaidya, A.B. (1998) Mitochondrial physiology as a target for atovaquone and other antimalarials. in *Malaria, Parasite Biology, Pathogenesis and Protection* (Sherman, I.W., ed.), pp. 355–368, ASM Press, Washington, DC
5. Van Dooren, G.G., Stimmler, L.M., and McFadden, G.I. (2006) Metabolic maps and functions of the *Plasmodium* mitochondrion. *FEMS Microbiol. Rev.* **30**, 596–630
6. Gardner, M.J., Hall, N., Fung, E., White, O., Berriman, M., Hyman, R.W., Carlton, J.M., Pain, A., Nelson, K.E., Bowman, S., Paulsen, I.T., James, K., Eisen, J.A., Rutherford, K., Salzberg, S.L., Craig, A., Kyes, S., Chan, M.S., Nene, V., Shallom, S.J., Suh, B., Peterson, J., Angiuoli, S., Pertea, M., Allen, J., Selengut, J., Haft, D., Mather, M.W., Vaidya, A.B., Martin, D.M., Fairlamb, A.H., Fraunholz, M.J., Roos, D.S., Ralph, S.A., McFadden, G.I., Cummings, L.M., Subramanian, G.M., Mungall, C., Venter, J.C., Carucci, D.J., Hoffman, S.L., Newbold, C., Davis, R.W., Fraser, C.M., and Barrell, B. (2002) Genome sequence of the human malaria parasite *Plasmodium falciparum*. *Nature* **419**, 498–511
7. Carlton, J.M., Angiuoli, S.V., Suh, B.B., Kooij, T.W., Pertea, M., Silva, J.C., Ermolaeva, M.D., Allen, J.E., Selengut, J.D., Koo, H.L., Peterson, J.D., Pop, M., Kosack, D.S., Shumway, M.F., Bidwell, S.L., Shallom, S.J., van Aken, S.E., Riedmuller, S.B., Feldblyum, T.V., Cho, J.K., Quackenbush, J., Sedegah, M., Shoaibi, A., Cummings, L.M., Florensk, L., Yatesk, J.R., Raine, J. D., Sinden, R.E., Harris, M.A., Cunningham, D.A., Preiser, P.R., Bergman, L.W., Vaidya, A.B., van Lin, L.H., Janse, C.J., Waters, A.P., Smith, H.O., White, O.R., Salzberg, S.L., Venter, J.C., Fraser, C.M., Hoffman, S.L., Gardner, M.J., and Carucci, D.J. (2002) Genome sequence and comparative analysis of the model rodent malaria parasite *Plasmodium yoelii yoelii*. *Nature* **419**, 512–519
8. Uyemura, S.A., Luo, S., Vieira, M., Moreno, S.N., and Docampo, R. (2004) Oxidative phosphorylation and rotenone-insensitive malate- and NADHquinone oxidoreductases in *Plasmodium yoelii yoelii* mitochondria *in situ*. *J. Biol. Chem.* **279**, 385–393
9. Matsushita, K., Ohnishi, T., and Kaback, H.R. (1987) NADH-ubiquinone oxidoreductases of the *Escherichia coli* aerobic respiratory chain. *Biochemistry* **26**, 7732–7737
10. Takeo, S., Kokaze, A., Ng, C.S., Mizuchi, D., Watanabe, J.I., Tanabe, K., Kojima, S., and Kita, K. (2000) Succinate dehydrogenase in *Plasmodium falciparum* mitochondria: molecular characterization of the *SDHA* and *SDHB* genes for the catalytic subunits, the flavoprotein (Fp) and iron–sulfur (Ip) subunits. *Mol. Biochem. Parasitol.* **107**, 191–205
11. Fry, M., Webb, E., and Pudney, M. (1990) Effect of mitochondrial inhibitors on adenosinetriphosphate levels in *Plasmodium falciparum*. *Comp. Biochem. Physiol. B* **96**, 775–782
12. Vaidya, A.B. and Mather, M.W.A. (2005) Post-genomic view of the mitochondrion in malaria parasites. *Curr. Top. Microbiol. Immunol.* **295**, 233–250
13. Painter, H.J., Morrisey, J.M., Mather, M.W., and Vaidya, A.B. (2007) Specific role of mitochondrial electron transport in blood-stage *Plasmodium falciparum*. *Nature* **446**, 88–91
14. Fry, M. and Pudney, M. (1992) Site of action of the antimalarial hydroxynaphthoquinone, 2-[trans-4-(4′-chlorophenyl)cyclohexyl]-3-hydroxy-1,4-naphthoquinone (566C80). *Biochem. Pharmacol.* **43**, 1545–1453
15. Biagini, G.A., Viriyavejakul, P., O'Neill, P.M., Bray, P.G., and Ward, S.A. (2006) Functional characterization and target validation of alternative Complex I of *Plasmodium falciparum* mitochondria. *Antimicrob. Agents Chemother.* **50**, 1841–1851
16. Srivastava, I.K., Rottenberg, H., and Vaidya, A.B. (1997) Atovaquone, a broad spectrum antiparasitic drug, collapses mitochondrial membrane potential in malarial parasite. *J. Biol. Chem.* **272**, 3961–3966
17. Uyemura, S.A., Luo, S., Moreno, S.N.J., and Docampo, R. (2000) Oxidative phosphorylation, $Ca^{2+}$ transport, and fatty acid-induced uncoupling in malaria parasites mitochondria. *J. Biol. Chem.* **275**, 9709–9715
18. Daily, J.P., Scanfeld, D., Pochet, N., Roch, K.L., Plouffe, D., Kamel, M., Sarr, O., Mboup, S., Ndir, O., Wypij, D., Lavasseur, K., Thomas, E., Tamayo, P., Dong, C., Zhou, Y., Lander, E.S., Ndiaye, D., Wirth, D., Winzeler, E.A., Mesirov, J.P., and Regev, A. (2007)

Distinct physiological states of *Plasmodium falciparum* in malaria-infected patients. *Nature* **450**, 1091–1095
19. Homewood, C.A. and Neame, K.D. (1976) Comparison of methods used for removal of white cells from malaria-infected blood. *Ann. Trop. Med. Parasitol.* **70**, 249–251
20. Takashima, E., Takamiya, S., Takeo, S., Mi-ichi, F., Amino, H., and Kita, K. (2001) Isolation of mitochondria from *Plasmodium falciparum* showing dihydroorotate dependent respiration. *Parasitol. Int.* **50**, 273–278
21. Johnson, D. and Lardy, H. (1967) Isolation of liver or kidney mitochondria in *Methods Enzymol.* Vol. 10, (Estabrook, R.W. and Pullman, M.E., eds.), pp. 94–96, Academic Press, New York
22. Mogi, T., Ui, H., Shiomi, K., Ōmura, S., and Kita, K. (2008) Gramicidin S identified as a potent inhibitor for cytochrome *bd*-type quinol oxidase. *FEBS Lett.* **582**, 2299–2302
23. Wittig, I., Karas, M., and Schagger, H. (2007) High resolution clear native electrophoresis for in-gel functional assays and fluorescence studies of membrane protein complexes. *Mol. Cell Proteomics* **6**, 1215–1122
24. Kobayashi, T., Sato, S., Takamiya, S., Komaki-Yasuda, K., Yano, K., Hirata, A., Onitsuka, A., Hata, M., Mi-ichi, F., Tanaka, T., Hase, T., Miyajima, A., Kawazu, S., Watanabe, Y., and Kita, K. (2007) Mitochondria and apicoplast of *Plasmodium falciparum*: behaviour on subcellular fractionation and the implication. *Mitochondrion* **7**, 125–132
25. Mi-Ichi, F., Miyadera, H., Kobayashi, T., Takamiya, S., Waki, S., Iwata, S., Shibata, S., and Kita, K. (2005) Parasite mitochondria as a target of chemotherapy: inhibitory effect of licochalcone A on the *Plasmodium falciparum* respiratory chain. *Ann. NY Acad. Sci.* **1056**, 46–54
26. Ueno, H., Miyoshi, H., Ebisui, K., and Iwamura, H. (1994) Comparison of the inhibitory action of natural rotenone and its stereoisomers with various NADH-ubiquinone reductases. *Eur. J. Biochem.* **225**, 411–417
27. Tushurashvili, P.R., Gavrikova, E.V., Ledenev, A.N., and Vinogradov, A.D. (1985) Studies on the succinate dehydrogenating system. Isolation and properties of the mitochondrial succinate-ubiquinone reductase. *Biochim. Biophys. Acta* **809**, 145–159
28. Miyadera, H., Shiomi, K., Ui, H., Yamaguchi, Y., Masuma, R., Tomoda, H., Miyoshi, H., Osanai, A., Kita, K., and Omura, S. (2003) Atpenins, potent and specific inhibitors of mitochondrial complex II (succinate-ubiquinone oxidoreductase). *Proc. Natl Acad. Sci. USA* **100**, 473–477
29. Suraveratum, N., Krungkrai, S.R., Leangaramgul, P., Prapunwattana, P., and Krungkrai, J. (2000) Purification and characterization of *Plasmodium falciparum* succinate dehydrogenase. *Mol. Biochem. Parasitol.* **105**, 215–222
30. Yankovskaya, V., Horsefield, R., Tornroth, S., Luna-Chavez, C., Miyoshi, H., Leger, C., Byrne, B., Cecchini, G., and Iwata, S. (2003) Architecture of succinate dehydrogenase and reactive oxygen species generation. *Science* **299**, 700–704
31. Sun, F., Huo, X., Zhai, Y., Wang, A., Xu, J., Su, D., Bartlam, M., and Rao, Z. (2005) Crystal structure of mitochondrial respiratory membrane protein complex II. *Cell* **121**, 1043–1057
32. Huang, L.S., Sun, G., Cobessi, D., Wang, A.C., Shen, J.T., Tung, E.Y., Anderson, V.E., and Berry, E.A. (2006) 3-Nitropropionic acid is a suicide inhibitor of mitochondrial respiration that, upon oxidation by Complex II, forms a covalent adduct with a catalytic base arginine in the active site of the enzyme. *J. Biol. Chem.* **281**, 5965–5972
33. Schägger, H. and Pfeiffer, K. (2000) Supercomplexes in the respiratory chains of yeast and mammalian mitochondria. *EMBO J.* **19**, 1777–1783
34. Kerscher, S.J. (2000) Diversity and origin of alternative NADH:ubiquinone oxidoreductase. *Biochim. Biophys. Acta* **1459**, 274–283
35. De Vries, S. and Grivell, L.A. (1988) Purification and characterization of a rotenone-insensitive NADH:$Q_6$ oxidoreductase from mitochondria of *Saccharomyces cerevisiae*. *Eur. J. Biochem.* **176**, 377–341
36. Björklöf, K., Zickermann, V., and Finel, M. (2000) Purifiction of the 45 kDa, membrane bound NADH dehydrogenase of *Escherichia coli* (NDH-2) and analysis of its interaction with ubiquinone analogs. *FEBS Lett.* **467**, 105–110
37. Kerscher, S.J., Okun, J.G., and Brandt, U. (1999) A single external enzyme confers alternative NADH:ubiquinone oxidoreductase activity in *Yarrowia lipolytica*. *J. Cell Sci.* **112**, 2347–2354
38. Rasmusson, A.G., Fredlund, K.M., and Møller, I.M. (1993) Purification of a rotenone-insensitive NAD(P)H dehydrogenase from the inner surface of red beetroot mitochondria. *Biochim. Biophys. Acta* **1141**, 107–110
39. Luethy, M.H., Thelen, J.J., Knudten, A.F., and Elthon, T.E. (1995) Purification, characterization, and submitochondrial localization of a 58-kilodalton NAD(P)H dehydrogenase. *Plant Physiol.* **107**, 443–450
40. Yamashita, T., Nakamaru-Ogiso, E., Miyoshi, H., Matsuo-Yagi, A., and Yagi, T. (2007) Roles of bound quinone in the single subunit NADH-quinone oxidoreductase (Ndi1) from *Saccharomyces cerevisiae*. *J. Biol. Chem.* **282**, 6012–6020
41. Miyoshi, H., Takegami, K., Sakamoto, K., Mogi, T., and Iwamura, H. (1999) Characterization of the ubiquinol oxidation sites in cytochromes *bo* and *bd* from *Escherichia coli* using aurachin C analogues. *J. Biochem.* **125**, 138–142
42. Yano, T., Li, L.-S., Weinstein, E., The, J.-S., and Rubin, H. (2006) Steady-state kinetics and inhibitory action of antitubercular phenothiazines on *Mycobacterium tuberculosis* type-II NADH-menaquinone oxidoreductase (NDH-2). *J. Biol. Chem.* **281**, 11456–11463
43. Roos, M.H. and Tielens, A.G.M. (1994) Differential expression of two succinate dehydrogenase subunit-B genes and a transition in energy metabolism during the development of the parasitic nematode *Haemonchus contortus*. *Mol. Biochem. Parasitol.* **66**, 273–281
44. Saruta, F., Kuramochi, T., Nakamura, K., Takamiya, S., Yu, Y., Aoki, T., Sekimizu, K., Kojima, S., and Kita, K. (1995) Stage-specific isoforms of complex II (succinate-ubiquinone oxidoreductase) in mitochondria from the parasitic nematode, *Ascaris suum*. *J. Biol. Chem.* **270**, 928–932
45. Morales, J., Mogi, T., and Kita, K. (2008) Divergence in structure of mitochondrial respiratory Complex II (succinate-ubiquinone reductase) revealed by protozoan enzymes. *Biochim. Biophys. Acta* **1777**, S94–S95
46. Oyedotun, K.S. and Lemire, B.D. (1999) The *Saccharomyces cerevisiae* succinate-ubiquinone oxidoreductase. Identification of Sdh3p amino acid residues involved in ubiquinone binding. *J. Biol. Chem.* **274**, 23956–23962
47. Krungkrai, J., Kanchanarithisak, R., Krungkrai, S.R., and Sunant Rochanakij, S. (2002) Mitochondrial NADH dehydrogenase from *Plasmodium falciparum* and *Plasmodium berghei*. *Exp. Parasitol.* **100**, 54–61
48. Vaidya, A.B., Painter, H.J., Morrisey, J.M., and Mather, M.W. (2008) The validity of mitochondrial dehydrogenases as antimalarial drug targets. *Trends Parasitol.* **24**, 8–9
49. Saleh, A., Friesen, J., Baumeister, S., Gross, G., and Bohne, W. (2007) Growth inhibition of *Toxoplasma gondii* and *Plasmodium falciparum* by nanomolar concentrations of 1-hydroxy-2-dodecyl-4(1*H*)quinolone, a high-affinity inhibitor of alternative (type II) NADH dehydrogenases. *Antimicrob. Agents Chemother.* **51**, 1217–1222
50. Eschemann, A., Galkin, A., Oettmeier, W., Brandt, U., and Kerscher, S. (2005) HDQ (1-hydroxy-2-dodecyl-4(1*H*)quinolone), a high affinity inhibitor for mitochondrial

alternative NADH dehydrogenase: evidence for a ping-pong mechanism. *J. Biol. Chem.* **280**, 3138–3142

51. Speijer, D., Breek, C.K., Muijsers, A.O., Hartog, A.F., Berden, J.A., Albracht, S.P., Samyn, B., van Beeumen, J., and Benne, R. (1997) Characterization of the respiratory chain from cultured *Crithidia fasciculate*. *Mol. Biochem. Parasitol.* **85**, 171–186
52. Nelson, R.E., Aphasizheva, I., Falick, A.M., Nebohacova, M., and Simpson, L. (2004) The I-complex in *Leishmania tarentolae* is an uniquely-structured $F_1$-ATPase. *Mol. Biochem. Parasitol.* **135**, 221–224
53. Minagawa, N., Yabu, Y., Kita, K., Nagai, K., Ohta, N., Meguro, K., Sakajo, S., and Yoshimoto, A. (1997) An antibiotic, ascofuranone, specifically inhibits respiration and in vitro growth of long slender bloodstream forms of *Trypanosoma brucei brucei*. *Mol. Biochem. Parasitol* **84**, 271–280
54. Saimoto, H., Shigemasa, Y., Kita, K., Yabu, Y., Hosokawa, T., and Yamamoto, M. (2007) Novel phenol derivatives and antitrypanosoma preventive/therapeutic agent comprising the same as active ingredient. U.S. Patent 20070208078

THE JOURNAL OF BIOLOGICAL CHEMISTRY VOL. 284, NO. 11, pp. 7255–7263, March 13, 2009


# Novel Mitochondrial Complex II Isolated from *Trypanosoma cruzi* Is Composed of 12 Peptides Including a Heterodimeric Ip Subunit*[S]

Received for publication, August 26, 2008, and in revised form, January 2, 2009 Published, JBC Papers in Press, January 2, 2009, DOI 10.1074/jbc.M806623200

**Jorge Morales[‡1], Tatsushi Mogi[‡2], Shigeru Mineki[§], Eizo Takashima[‡3], Reiko Mineki[¶], Hiroko Hirawake[‡], Kimitoshi Sakamoto[‡], Satoshi Ōmura[‖], and Kiyoshi Kita[‡4]**

*From the [‡]Department of Biomedical Chemistry, Graduate School of Medicine, the University of Tokyo, Hongo, Bunkyo-ku, Tokyo 113-0033, the [§]Department of Applied Biological Science, Faculty of Science and Technology, Tokyo University of Science, Noda, Chiba 278-8510, the [¶]Division of Proteomics and BioMolecular Science, Juntendo University Graduate School of Medicine, Hongo, Bunkyo-ku, Tokyo 113-8421, and the [‖]Kitasato Institute for Life Sciences and Graduate School of Infection Control Sciences, Kitasato University, Minato-ku, Tokyo 108-8641, Japan*

**Mitochondrial respiratory enzymes play a central role in energy production in aerobic organisms. They differentiated from the α-proteobacteria-derived ancestors by adding non-catalytic subunits. An exception is Complex II (succinate: ubiquinone reductase), which is composed of four α-proteobacteria-derived catalytic subunits (SDH1–SDH4). Complex II often plays a pivotal role in adaptation of parasites in host organisms and would be a potential target for new drugs. We purified Complex II from the parasitic protist *Trypanosoma cruzi* and obtained the unexpected result that it consists of six hydrophilic (SDH1, $SDH2_N$, $SDH2_C$, and SDH5–SDH7) and six hydrophobic (SDH3, SDH4, and SDH8–SDH11) nucleus-encoded subunits. Orthologous genes for each subunit were identified in *Trypanosoma brucei* and *Leishmania major*. Notably, the iron-sulfur subunit was heterodimeric; $SDH2_N$ and $SDH2_C$ contain the plant-type ferredoxin domain in the N-terminal half and the bacterial ferredoxin domain in the C-terminal half, respectively. Catalytic subunits (SDH1, $SDH2_N$ plus $SDH2_C$, SDH3, and SDH4) contain all key residues for binding of dicarboxylates and quinones, but the enzyme showed the lower affinity for both substrates and inhibitors than mammalian enzymes. In addition, the enzyme binds protoheme IX, but SDH3 lacks a ligand histidine. These unusual features are unique in the Trypanosomatida and make their Complex II a target for new chemotherapeutic agents.**

The parasitic protist *Trypanosoma cruzi* is the etiological agent of Chagas disease, a public health threat in Central and South America. These parasites are normally transmitted by reduviid bugs via the vector feces after a bug bite and also via transfusion of infected blood. About 16–18 million people are infected, and 100 million are at risk, but there are no definitive chemotherapeutic treatments available (1). Despite having potential pathways for oxidative phosphorylation (2), all trypanosomatids (*Trypanosoma* and *Leishmania* species) analyzed so far are characterized by incomplete oxidation of glucose with secretion of end products, such as succinate, alanine, ethanol, acetate, pyruvate, and glycerol (3, 4) (Fig. 1). Major routes for formation of succinate in *Trypanosoma brucei* are via NADH-dependent fumarate reductase in glycosomes and mitochondria (5, 6). In trypanosomatid mitochondria, the Krebs cycle is inefficient, and pyruvate is principally converted to acetate via acetate:succinate CoA transferase (7). A part of the Krebs cycle operates the utilization of histidine in the insect stage of *T. cruzi* (8).

Mitochondrial Complex II (succinate:quinone reductase (SQR)[5] and succinate dehydrogenase (SDH)) serves as a membrane-bound Krebs cycle enzyme and often plays a pivotal role in adaptation of parasites to environments in their host (9, 10). In general, Complex II consists of four subunits (11). A flavoprotein subunit (SDH1, Fp) and an iron-sulfur subunit (SDH2, Ip) form a soluble heterodimer, which then binds to a membrane anchor heterodimer, SDH3 (CybL) and SDH4 (CybS). SDH1 contains a covalently bound FAD and catalyzes the oxidation of succinate to fumarate. SDH2 transfers electrons to ubiquinone via the [2Fe-2S] cluster in the N-terminal plant-type ferredoxin domain ($Ip_N$) and the [4Fe-4S] and [3Fe-4S] clusters in the C-terminal bacterial ferredoxin domain ($Ip_C$). Ubiquinone is bound and reduced in a pocket provided by SDH2, SDH3, and SDH4 (12–14). SDH3 and SDH4 contain three transmembrane helices and coordinate protoheme IX via histidine in the second helices of each subunit (11–14).

* This work was supported in part by Grant-in-aid for Scientific Research 20570124 (to T. M.), Creative Scientific Research Grant 18GS0314 (to K. K.), Grant-in-aid for Scientific Research on Priority Areas 18073004 (to K. K.) from the Japanese Society for the Promotion of Science, and Targeted Proteins Research Program (to K. K.) from the Japanese Ministry of Education, Science, Culture, Sports and Technology (MEXT). The costs of publication of this article were defrayed in part by the payment of page charges. This article must therefore be hereby marked "*advertisement*" in accordance with 18 U.S.C. Section 1734 solely to indicate this fact.

[S] The on-line version of this article (available at http://www.jbc.org) contains supplemental Table S1.

[1] Supported by a Japanese Government scholarship from Ministry of Education, Science, Culture, Sports and Technology.

[2] To whom correspondence may be addressed. Tel.: 81-3-5841-3526; Fax: 81-3-5841-3444; E-mail: tmogi@m.u-tokyo.ac.jp.

[3] Present address: Dept. of Microbiology, School of Life Dentistry at Tokyo, Nippon Dental University, Tokyo 102-8159, Japan.

[4] To whom correspondence may be addressed. Tel.: 81-3-5841-3526; Fax: 81-3-5841-3444; E-mail: kitak@m.u-tokyo.ac.jp.

[5] The abbreviations used are: SQR, succinate:quinone reductase; hrCNE, high resolution clear native electrophoresis; $IC_{50}$, the 50% inhibitory concentration; $Ip_N$, the N-terminal plant-type ferredoxin domain; $Ip_C$, the C-terminal bacterial ferredoxin domain; DCIP, 2,4-dichlorophenolindophenol; SML, sucrose monolaurate; Tricine, *N*-[2-hydroxy-1,1-bis(hydroxymethyl)ethyl]-glycine; MOPS, 3-(*N*-morpholino)propanesulfonic acid; $Q_n$, ubiquinone-*n*.

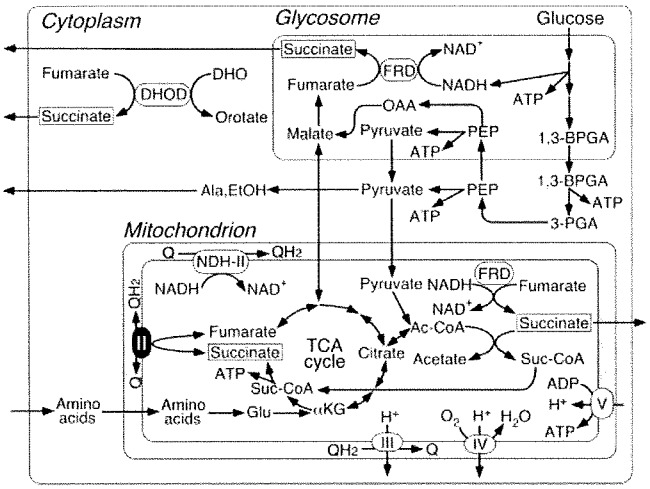


FIGURE 1. **Metabolic pathways in *T. cruzi*.** Incomplete oxidation of glucose takes place in glycosomes and mitochondria, and end products such as succinate, L-alanine, ethanol, and acetate are excreted from parasites (3, 4). Cytoplasmic dihydroorotate (*DHO*):fumarate reductase (*DHOD*) contributes succinate production (6).

Parasitic nematodes adapted to hypoxic host environments often have modified respiratory chains. Many adult parasites perform fumarate respiration by expressing a stage-specific isoform of Complex II (9, 10). *Hemonchus contortus* uses an isoform for SDH2 (9), whereas *Ascaris suum* uses isoforms for SDH1 and SDH4 (10). To explore the adaptive strategy in a parasitic protist, we isolated mitochondria from axenic culture of *T. cruzi* epimastigotes and characterized the purified Complex II. Our results demonstrated for the first time that *T. cruzi* Complex II is an unusual supramolecular complex with a heterodimeric iron-sulfur subunit and seven novel noncatalytic subunits. Purified enzyme showed reduced binding affinities for both substrates and inhibitors. Because this novel structural organization is conserved in all trypanosomatids (2, 15, 16), parasite Complex II would be a potential target for the development of new chemotherapeutic agents for trypanosomiasis and leishmaniasis.

## EXPERIMENTAL PROCEDURES

*Preparation of Mitochondria*—*T. cruzi* strain Tulahuhen was grown statically for 6–7 days at 26 °C in 300-$cm^2$ cell culture flasks (Falcon, BD Biosciences) containing 250 ml of the modified LIT medium (17), supplemented with 0.1% (w/v) glucose, 0.001% (w/v) hemin (Sigma), and 5% (v/v) fetal bovine serum (MP Biochemicals). Mitochondria were isolated from epimastigotes by the differential centrifugation method (18) with slight modifications. Parasites grown to $6-8 \times 10^7$ cells/ml were washed with buffer A (20 mM Tris-HCl, pH 7.2, 10 mM $NaH_2PO_4$, 1 mM sodium EDTA, 1 mM dithiothreitol, 0.225 M sucrose, 20 mM KCl, and 5 mM $MgCl_2$). Cells were disrupted by grinding with silicon carbide (Carborundum 440 mesh; Nacalai Tesque, Kyoto, Japan) in the presence of a minimum volume of buffer B (25 mM Tris-HCl, pH 7.6, 1 mM dithiothreitol, 1 mM sodium EDTA, 0.25 M sucrose, and EDTA-free Complete protease inhibitor mixture (Roche Applied Science)). The resultant cell paste was resuspended in buffer B and centrifuged at 500 × *g* for 5 min and 1000 × *g* for 15 min to remove silicon carbide and nuclear fraction, respectively. The mitochondrial fraction was recovered upon centrifugation of the last supernatant at 10,000 × *g* for 15 min, washed three times in buffer B, and resuspended to a protein concentration of ~30 mg/ml and kept at −80 °C until use.

**TABLE 1**
**Purification of complex II from *T. cruzi* mitochondria**

| Step | Protein | Succinate:DCIP reductase | Yield | Purification |
|---|---|---|---|---|
| | *mg* | *units* | *units/mg* | % | *-fold* |
| Mitochondria | 314 | 27 | 0.085 | 100 | 1.0 |
| SML extract | 141 | 22 | 0.16 | 83 | 1.9 |
| Source 15Q | 7.8 | 7.6 | 0.97 | 28 | 12 |
| Superdex 200 (1st) | 1.3 | 1.4 | 1.09 | 5.3 | 13 |
| Superdex 200 (2nd) | 0.15 | 0.43 | 2.87 | 1.6 | 34 |

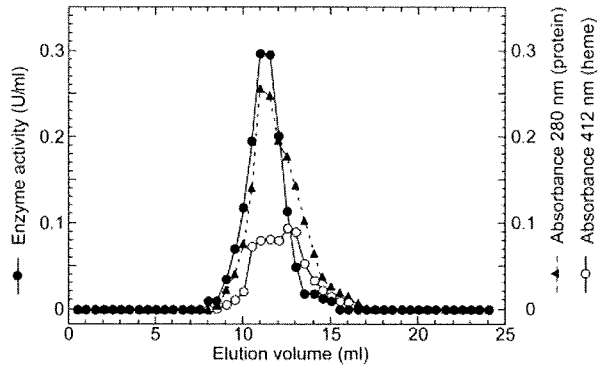


FIGURE 2. **Elution profile of *T. cruzi* Complex II on Superdex 200 chromatography.** Complex II fractions from the first gel filtration chromatography with a Superdex 200-pg column were concentrated and rechromatographed at the flow rate of 0.25 ml/min. Aliquots were collected every 0.5 ml. Elution profiles for proteins and cytochromes were monitored at 280 (▲) and 412 nm (○), respectively, and the enzyme activity (●) was measured as decylquinone-mediated succinate:DCIP reductase.

*Isolation of Complex II*—All steps were carried out at 4 °C. Mitochondrial fraction (~300 mg of protein from 10 liters culture) was brought to 70 ml with buffer C (10 mM $KP_i$, pH 7.5), 1 mM sodium EDTA, 1 mM sodium malonate, EDTA-free Complete protease inhibitor mixture (Roche Applied Science) (2 tablets/50 ml), 1% (w/v) sucrose monolaurate SM-1200 (SML) (Mitsubishi-Kagaku Foods Co., Tokyo, Japan)). The mixture was stirred for 30 min and centrifuged at 200,000 × *g* for 1 h. The supernatant was loaded at 1 ml/min onto a Source 15 Q column (1.6 inner diameter × 10 cm; GE Healthcare), equilibrated with buffer C containing 0.1% SML. After washing with 5 volumes of the same buffer, proteins were eluted with a 200-ml linear gradient of NaCl from 0 to 150 mM at 2 ml/min. Active fractions were concentrated to ~250 μl by ultrafiltration with Amicon Ultra-4 (molecular weight cutoff 100,000, Millipore) and subjected to gel filtration FPLC with a Superdex 200-pg 10/300 GL column (1 cm inner diameter × 30 cm; GE Healthcare) at 0.25 ml/min in 20 mM MOPS-NaOH, pH 7.2, containing 1 mM sodium EDTA, 1 mM sodium malonate, 150 mM NaCl, and 0.1% SML. Peak fractions were rechromatographed as above, and purified enzyme was concentrated and stored at −80 °C until use.

*Identification of Complex II Subunits*—The purified enzyme was subjected to 12.5% SDS-PAGE, and subunits were transferred to an Immobilon-P membrane (Millipore), followed by

staining with Coomassie Brilliant Blue R-250 (19, 20). Five or ten N-terminal amino acid residues were determined with a Procise 494 HT (Applied Biosystems) or an Hp G1005A (Hewlett-Packard Co.) Protein Sequencing System at the Bio-Medical Research Center of Juntendo University or APRO Life Science Institute, Inc. (Tokushima, Japan). When the N terminus was blocked, protein bands were digested with trypsin, and internal peptide sequences were determined (20). Genes coded for Complex II subunits were identified with BLASTP in the *T. cruzi* genome data base (15).

*Phase Partitioning of Mitochondrial Fraction with Triton X-114*—Phase partitioning by Triton X-114 was performed as described previously (21) with a slight modification. A total of 2–3 mg of mitochondrial fraction was resuspended in 1 ml of Tris-HCl, pH 7.5, 150 mM NaCl, 1 mM EDTA, 2 mM sodium malonate, Complete protease inhibitors mixture (Roche Applied Science) (2 tablets/50 ml), protease inhibitors mixture for mammalian cell and tissue extracts (Sigma) (10 μl/ml), and 2% (v/v) Triton X-114. The mixture was incubated for 30 min on ice and kept at −30 °C overnight. After thawing, the insoluble material was removed by centrifugation at 4 °C, and the supernatant was incubated for 10 min at 37 °C and centrifuged at 2000 × *g* for 10 min to separate the aqueous and detergent-rich phases. The aqueous phase was brought to 2% (v/v) Triton X-114, whereas the detergent-rich fraction was brought to 1 ml with the above buffer. After incubation on ice for 10 min, samples were incubated at 37 °C for 10 min and phases separated as before. This wash step was repeated three times. Finally, the samples were dialyzed and concentrated by Amicon Ultra-4 (Millipore) in the presence of 50 mM imidazole, 50 mM NaCl, 6 mM aminocaproic acid, 0.05% (w/v) deoxycholate, and 0.1% (w/v) SML, pH 7, and kept at −80 °C until use.

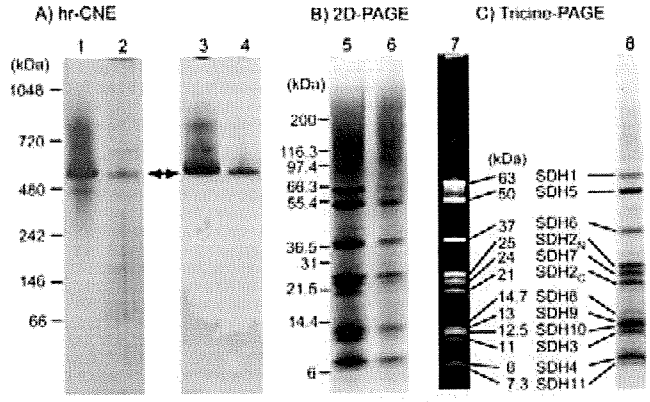


FIGURE 3. **Electrophoresis analysis of *T. cruzi* Complex II.** *A*, purified Complex II (2 μg; *lanes 1* and *3*) and the detergent-rich fraction from the phase partitioning by Triton X-114 of the mitochondrial fraction (60 μg; *lines 2* and *4*) were subjected to hrCNE. Proteins were stained by Coomassie Brilliant Blue (*left panel*), and Complex II was visualized by SDH activity staining (*right panel*). *B*, proteins of Complex II showing SDH activity in *A* were analyzed by 10–20% Tricine SDS-PAGE and visualized by silver stain (*lane 5*, pure complex; *lane 6*, detergent-rich fraction). *C* shows the subunit composition of the pure Complex II from *T. cruzi* stained by SYPRO ruby (*lane 7*) or silver stain (*lane 8*). Molecular weight standards used are NativeMark (Invitrogen, *lane 1*) and Mark 12 unstained standards (Invitrogen, *lanes 5* and *7*).

*Enzyme Assay*—Decylubiquinone-mediated succinate-2,4 dichlorophenolindophenol (DCIP) reductase activity was measured at 25 °C in 100 mM potassium phosphate, pH 7.4, containing 1 mM $MgCl_2$, 2 mM KCN, 0.1 mM antimycin A (Sigma), and 0.1% SML with 63 μM decylubiquinone (Sigma) *plus* 60 μM DCIP. After 2 min of incubation, reduction of DCIP ($\epsilon_{600}$ = 21 $mM^{-1}$ $cm^{-1}$) was measured in the presence of 10 mM succinate. SQR activity was determined with 40 μM ubiquinone-2 ($Q_2$) (Sigma, $\epsilon_{278}$ = 12.3 $mM^{-1}$ $cm^{-1}$). Kinetic analysis was done with KaleidaGraph version 4.0 (Synergy Software).

*Miscellaneous*—High resolution clear native electrophoresis (hrCNE) (22) was performed with 4–16% Novex gels (Invitrogen) using 0.02% dodecylmaltoside and 0.05% sodium deoxycholate for the cathode buffer additives, and the Complex II band was visualized by the activity staining (23) or Coomassie Brilliant Blue. Tricine-PAGE analysis was done with Novex 10–20% Tricine gels (Invitrogen), and proteins bands were sequentially stained by Sypro ruby (Invitrogen) and silver. During purification the succinate-decylubiquinone-DCIP reduc-

**TABLE 2**
**Identification of genes encoding subunits for *T. cruzi* complex II**

| Subunit[a] | Sequence confirmed[b] | Accession number or RefSeq ID at NCBI (haplotype,[c] $M_r$) | Identity[d] | TM[e] |
|---|---|---|---|---|
| | | | % | |
| SDH1 | $Ser^{10}$–$Met^{19}$ | AB031741 (NE, 66,974), XP_809281 (E, 18,231) | 59 | 0 |
| SDH5 | $Ala^{10}$–$Leu^{19}$ | XP_818124 (NE, 53,831), XP_810172 (E, 20,788) | 16 | 0 |
| $SDH2_N$ | $Ser^{188}$–$Arg^{196}$, $Lys^{201}$–$Ile^{204}$, $Gly^{221}$–$Asn^{223}$, $Glu^{267}$–$Ile^{269}$ | XP_814994 (merged, 32,232)[f] | 24 (37) | 0 |
| $SDH2_C$ | $Pro^{2}$–$Leu^{6}$ | XP_803796 (NE, 21,352), XP_806126 (E, 21,379) | 25 (43) | 0 |
| SDH6a | $Val^{19}$–$Val^{28}$ | XP_809065 (NA, 36,077), XP_812789 (NA, 36,035) | 15 | 0 |
| SDH6b | $Val^{19}$–$Val^{28}$ | XP_813603 (NA, 36,133), XP_813645 (NA, 36,039) | 14 | 0 |
| SDH7 | $Ile^{26}$–$Leu^{35}$ | XP_813318 (NE, 28,218), XP_820239 (E, 28,202) | 22 | 0 |
| SDH3 | $Val^{2}$–$Phe^{11}$ | XP_809410 (NE, 12,176), XP_810064 (E, 12,204) | 29 | 1 |
| SDH4 | $Phe^{39}$–$Thr^{48}$ | XP_808211 (E, 13,957), XP_816430 (NE, 13,975) | 27 | 2 |
| SDH8 | $Gly^{5}$–$Met^{16}$ | XP_809192 (NE, 16,199), XP_817545 (E, 16,143) | ND[g] | 2 |
| SDH9 | $Ile^{10}$–$Pro^{19}$ | XP_807105 (merged, 15,736) | ND | 1 |
| SDH10 | $Pro^{25}$–$Val^{33}$ | XP_808894 (NE, 15,565), XP_808903 (E, 15,554) | ND | 1 |
| SDH11 | $Phe^{20}$–$Cys^{29}$ | XP_814088 (E, 10,346), XP_814509 (NE, 10,337) | ND | 1 |

[a] Alleles were named as SDH3-1 (XP_809410) and SDH3-2 (XP_810064) in the order of the accession numbers, except for SDH5.
[b] These are N-terminal sequences except for $SDH2_N$ and SDH8, where the N-terminal residues were blocked.
[c] Homozygous alleles located in a merged assembly of Esmeraldo (E) and non-Esmeraldo (NE) homologous sequences whose different copies were merged genes during the genome assembly are indicated by "merged." Haplotypes for gene with more than two copies in the genome that does not belong to a merged region are not assigned (NA).
[d] Identity % to counterparts in human were as follows: SDH1 (D30648), SDH2 (P21912), SDH3 (Q99643), or SDH4 (O14521). In parentheses, the identity % of $SDH2_N$ and $SDH2_C$ that correspond to either $Met^{1}$–$Pro^{155}$ ($Ip_N$ domain) or $Tyr^{156}$–$Val^{280}$ ($Ip_C$ domain), respectively, of human SDH2 is shown. Identity % for truncated forms of SDH1 and SDH5 (SDH1-2 and SDH5-2) in the Esmeraldo haplotype was 66 and 20%, respectively.
[e] Transmembrane segments (TM) were estimated with TMHMM (52) and SOSUI (53).
[f] SDH2N from other trypanosomatids lack $Met^{1}$ to $Arg^{42}$ of $TcSDH2_N$.
[g] ND indicates not determined because these hydrophobic sequences are a highly divergent form of mammalian sequences.

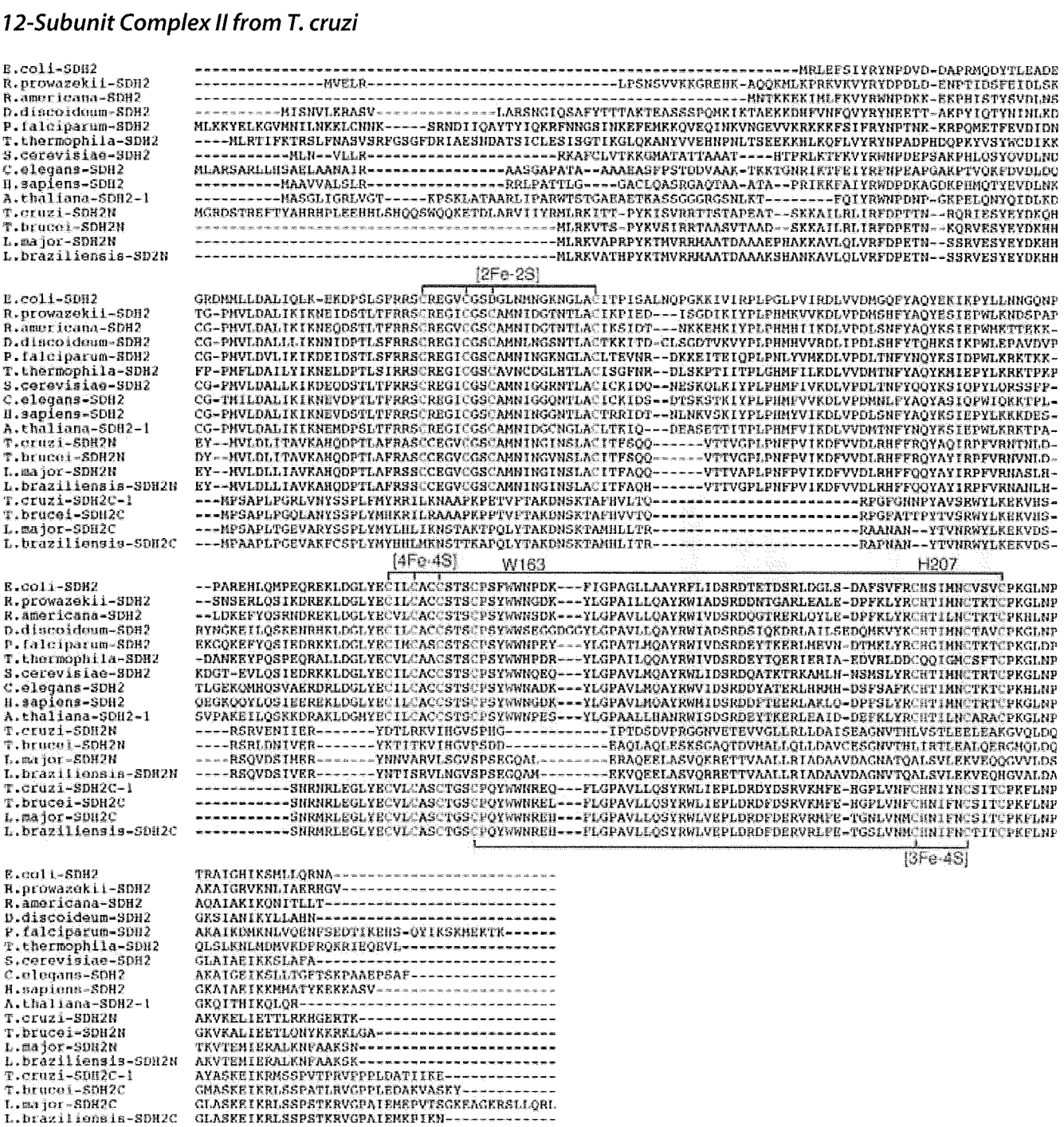


FIGURE 4. **Alignment of heterodimeric SDH2 sequences.** Amino acid residues proposed for binding of the iron-sulfur clusters are shown in *red* and those for the quinone binding in *blue*. Residue numbers refer to the *E. coli* SDH2 (SdhB) sequence. GenBank™ accession numbers for $SDH2_N$ and $SDH2_C$ sequences used are *T. cruzi* (XP_814994 and XP_803796), *T. brucei* (XP_847169 and XP_826981), and *L. major* (XP_001683488 and XP_001682013). Other SDH2 sequences used are *E. coli* (NP_415252), *Rickettsia prowazekii* (Q9ZEA1), *Reclinomonas americana* (NP_044798), *Dictyostelium discoideum* (XP_646559), *Plasmodium falciparum* (D86574), *Tetrahymena thermophila* (XP_001024894), *S. cerevisiae* (NP_012774), *Caenorhabditis elegans* (NP_495992), *H. sapiens* (NP_002991), and *A. thaliana* (NP_189374).

tase activity was monitored in a microplate spectrophotometer (Benchmark Plus, Bio-Rad). Kinetics and UV-visible absorption spectra were determined at room temperature with a V-660 UV-visible spectrophotometer (Jasco, Tokyo, Japan). Protoheme IX and protein concentrations were determined by pyridine hemochromogen method (24) and the micro BCA method (Pierce), respectively. Sequence alignment was done with ClustalX 2.0 (25).

## RESULTS AND DISCUSSION

*Isolation of T. cruzi Complex II*—To determine the molecular organization of *T. cruzi* Complex II, we purified this enzyme from epimastigote mitochondria by ion-exchange and gel filtration chromatography using the nonionic detergent sucrose monolaurate (Table 1). Decylubiquinone-mediated succinate: DCIP reductase activity was eluted as a single peak at each step

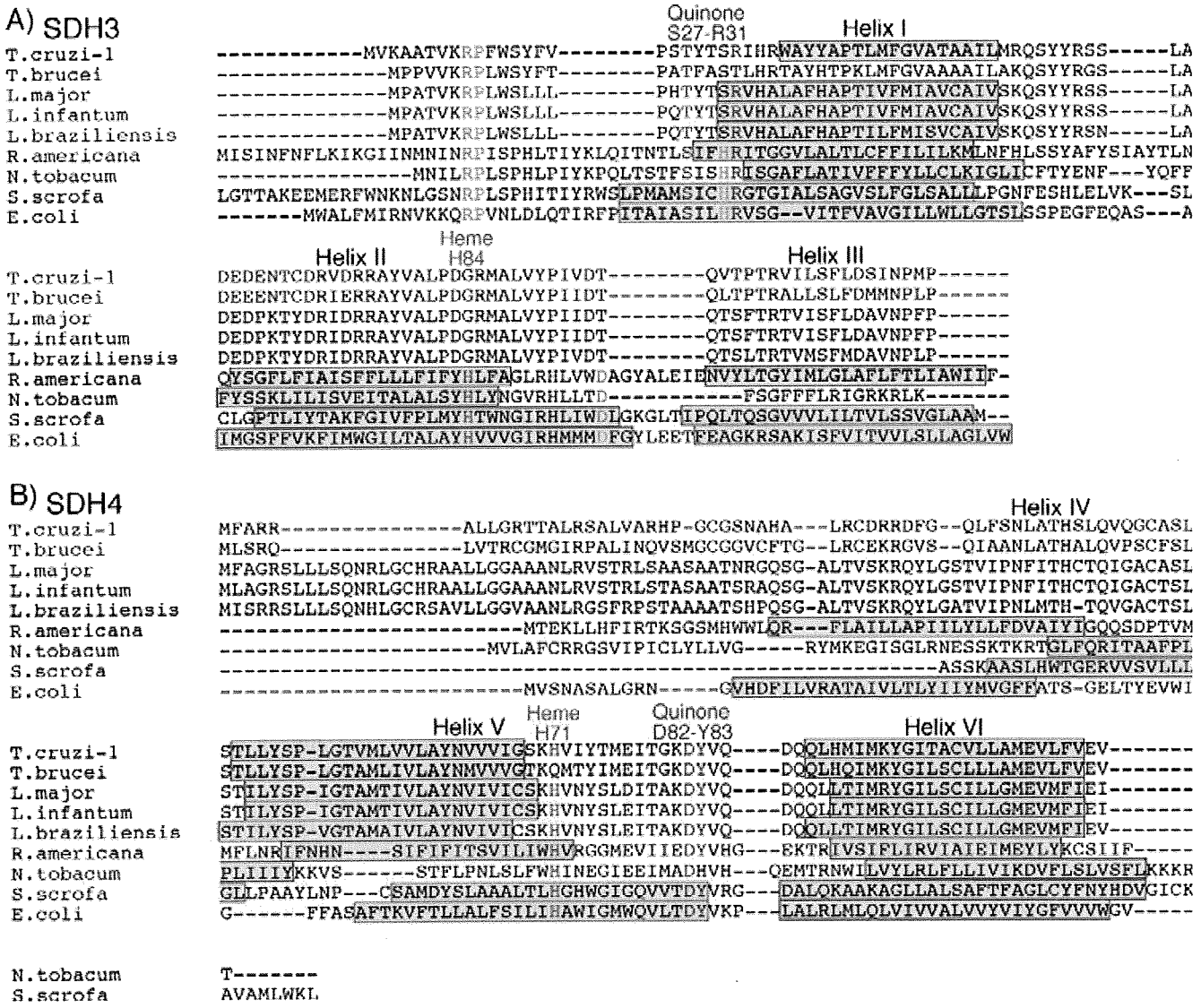


FIGURE 5. **Alignments of SDH3 (*A*) and SDH4 (*B*) sequences.** Amino acid residues proposed for binding of protoheme IX are shown in *red* and those for the quinone binding in *blue*. Other conserved residues are indicated by *green*. Transmembrane helices found in *E. coli* (Protein Data Bank code 1NEK) and porcine (Protein Data Bank code 1ZOY) Complex II are shown by *red rectangles*, and transmembrane helices predicted by TMHMM are indicated by *blue rectangles*. TMHMM failed to predict transmembrane helices in *T. brucei* SDH3. Residue numbers refer to *E. coli* SDH3 (SdhC) and SDH4 (SdhD). GenBank™ accession numbers for SDH3 and SDH4 sequences used are *T. cruzi* (XP_809410, XP_808211), *T. brucei* (XP_845531, XP_823384), *L. major* (XP_001684890, XP_001685874), *L. infantum* (XP_001467132), *L. brasiliensis* (XP_001566908, XP_001567905), *R. americana* (NP_044796, NP_044797), *Nicotiana tobacum* (YP_173376, YP_173457), *Sus scrofa* (1ZOY_C, 1ZOY_D), and *E. coli* (NP_415249, NP_415250).

and co-eluted with proteins and *b*-type cytochrome(s) at the second Superdex 200 chromatography (Fig. 2). Specific activity was increased 34-fold to 2.9 units/mg proteins, and the yield was ~2%. A hrCNE of the pure protein identified *T. cruzi* Complex II as an ~550-kDa complex (Fig. 3, *lanes 1* and *3*), which is 4-fold larger than bovine and yeast Complex II (130 kDa) and potato Complex II (150 kDa) (26, 27). Upon phase partitioning of the mitochondrial fraction with Triton X-114, the Complex II of *T. cruzi* was found only in the detergent-rich fraction (data not shown). Analysis of the detergent-rich fraction by hrCNE showed the Complex II as a single band at the same position as the pure enzyme (~550 kDa) (Fig. 3, *lanes 2* and *4*). These results indicated that the purified Complex II was obtained in its intact form. Interestingly, second dimensional analysis of both the purified Complex II and the detergent-rich fraction from phase partitioning with Triton X-114 with SDH activity showed that *T. cruzi* Complex II is composed of 12 subunits (Fig. 3, *lanes 5* and *6*). The same subunit composition was obtained by immunoaffinity purification of the partially purified enzyme (data not shown). The apparent molecular weight of the subunits ranges from 7.3 to 63 kDa (Fig. 3, *lanes 7* and *8*). Assuming the presence of equimolar amounts of subunits, a total molecular mass of Complex II would be 286.5 kDa, indicating that *T. cruzi* Complex II is a homodimer.

*Identification of Genes Coded for Subunits*—We determined N-terminal sequences (or internal peptide sequences in case of $SDH2_N$ and SDH8) of all subunits and identified genes coded for SDH1-1, $SDH2_N$, $SDH2_C$, SDH5–SDH7 (hydrophilic sub-

units), SDH3, SDH4, and SDH8–SDH11 (hydrophobic subunits) (Table 2). All subunits, except SDH1-1, are trypanosomatid-specific and structurally unrelated to plant-specific soluble subunits (AtSDH5–AtSDH8, 5–18 kDa) (27–29). All genes (except SDH6 with four copies) are present as two copies, which are assigned to either Esmeraldo or non-Esmeraldo haplotype (haploid genotype) in *T. cruzi* subgroup IIe. In contrast, only one copy each of the orthologues is present in *T. brucei*, *Leishmania major*, *Leishmania infantum*, and *Leishmania braziliensis* (supplemental Table S1). N-terminal sequence analysis of SDH3 and SDH7 showed that yields of two isoforms are similar (*i.e.* SDH3-1:SDH3-2 = 63:37, and SDH7-1:SDH7-2 = 54:46), indicating that isoforms are expressed from each haplotype. Because truncated isoforms for SDH1 and SDH5 in the Esmeraldo haplotype (see below) are not assembled into the 12-subunit complex and $SDH2_N$ and SDH9 isoforms have the identical sequence, 512 ($= 1^4 \times 4^1 \times 2^{(12-5)}$) kinds of heterogeneity may exist in the *T. cruzi* Complex II monomer (Table 2).

*Flavoprotein Subunit*—SDH1-1 (63-kDa band in Tricine-PAGE) cross-reacted with the antiserum against bovine SDH1 (data not shown) and is highly homologous to counterparts in *T. brucei* (93% identity), *L. major* (90%), *Homo sapiens* (59%), *Arabidopsis thaliana* (62%), *Saccharomyces cerevisiae* (61%), and *Escherichia coli* (48%, SdhA). Amino acid residues proposed for dicarboxylate binding and a FAD ligand histidine (12–14) are all conserved in SDH1-1. SDH1-1 and SDH5-1 of the non-Esmeraldo haplotype share a weak sequence similarity in the entire region, but the latter lacks amino acid residues responsible for FAD and dicarboxylate binding. In the Esmeraldo haplotype, SDH1-2 and SDH5-2 are truncated and contain only $Met^1$ to $Gly^{167}$ of TcSDH1-1 and $Ile^{305}$ to $Met^{486}$ of TcSDH5-1, respectively (Table 2). These findings suggest that TcSDH1-1, TcSDH1-2, TcSDH5-1, and TcSDH5-2 might have evolved by gene duplication and subsequent degeneration.

*Iron-Sulfur Subunit*—Sequence analysis of the 25- and 21-kDa band proteins revealed that they contain the plant ferredoxin domain ($Ip_N$) and bacterial ferredoxin domain ($Ip_C$) of canonical SDH2 (Ip) in the N- and C-terminal half, respectively (Fig. 4). Sequence identities of $Ip_N$ and $Ip_C$ are 37 and 43%, respectively, to those of human SDH2 (Table 2), and the $Ip_N$ and $Ip_C$ domains contain all amino acid residues responsible for binding of iron-sulfur clusters and ubiquinone (12, 13, 30) (Fig. 4). Such a heterodimeric Ip subunit can be found in *T. brucei* (31), *T. cruzi*, *L. major*, *L. infantum*, and *L. brasiliensis* (Tables 2), which belong to the order Trypanosomatida. Thus we named these subunits as $SDH2_N$ and $SDH2_C$, respectively.

Splitting of mitochondrial membrane proteins has been reported for cytochrome *c* oxidase CoxII in Apicomplexa and Chlorophyceae (32, 33), and ATP synthase $\alpha$ subunit in *Leishmania tarentolae* and *T. brucei* (34, 35). The former occurs at the gene level and the latter by post-translational cleavage. Sequence analysis indicates that heterodimeric SDH2 and CoxII have emerged from gene duplication followed by degeneration of the N- or C-terminal half of the duplication products. Conserved domains in degenerated duplicons, which have arisen from mitochondrion-to-nucleus transfer of the duplicated genes (32, 33, 36), must retain the potential for protein-protein interactions and constitute a heterodimeric functional subunit by trans-complementation.

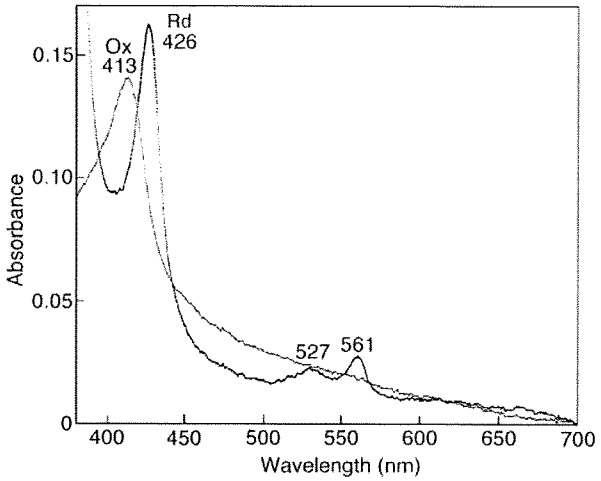


FIGURE 6. **Visible absorption spectra of *T. cruzi* Complex II.** Purified Complex II was desalted by ultrafiltration and diluted with 0.1 M sodium phosphate, pH 7.2, containing 0.1% SML at a final concentration of 0.06 mg/ml. Absorption spectra of the air-oxidized (*Ox, thin line*) and dithionite-reduced (*Rd, thick line*) forms were recorded at room temperature with UV-2400 spectrophotometer (Shimadzu Corp., Kyoto, Japan).

*Membrane Anchor Subunits*—Membrane anchor subunits in protist enzymes are highly divergent from bacterial and mammalian counterparts and difficult to find with conventional BLAST programs. We identified candidates for *T. cruzi* SDH3 and SDH4 by the presence of the quinone/heme-binding motifs "$RPX_{16}SX_2HR$ (SDH3 helix I)" and "$HX_{10}DY$ (SDH4 helix V)," respectively, present in membrane anchor subunits. In Complex II, $Trp^{164}$ in SDH2 (Fig. 4) and $Tyr^{83}$ in the SDH4 $HX_{10}DY$ motif (Fig. 5*B*) (*E. coli* numbering) could hydrogen bond to the O-1 atom of ubiquinone and contribute to the binding affinity (12, 37). $Arg^{31}$ in the SDH3 $SX_2HR$ motif (Fig. 5*A*) and $Asp^{82}$ in the SDH4 $HX_{10}DY$ motif are in close proximity to ubiquinone and could interact with $Tyr^{83}$ (37). $Ser^{27}$ in the SDH3 $SX_2HR$ motif has been shown to be essential for quinone binding (38) and is a candidate for hydrogen bonding to the O-4 atom of ubiquinone (30). The first arginine ($Arg^9$ in *E. coli* SDH3) in the $RPX_{16}SX_3R$ motif is in the vicinity of $Glu^{186}$ in SDH1 and $Asp^{106}$ in SDH2 and may play a structural role by making a hydrogen bond network.

In *T. cruzi*, SDH3 has the "$RPX_{11}SX_2HR$ motif in front of the predicted transmembrane helix I and lacks transmembrane helices II and III. However, sequence alignment suggests the presence of the alternative motif "$TX_2SR/(T)$" in the Trypanosomatida (Fig. 5*A*). In mitochondrial Complex II, protoheme IX is ligated by two His residues in the second transmembrane helix of SDH3 ("$HX_{10}D$" motif) and SDH4 ("$HX_{10}DY$" motif). A heme ligand in helix II ($His^{84}$ in *E. coli* SDH3) may be substituted by a nearby histidine in the quinone-binding motif "$SX_2HR$" (39). In contrast, SDH4 lacks helix IV and appears to interact with heme and ubiquinone with the $HX_{10}DY$ motif. As in rice SDH4 (GenBank™ accession number NP_001045324), the heme ligand His is substituted by Gln in *T. brucei* SDH4. The presence of a bound heme or an alternative ligand in *T.*

*brucei* SDH4 needs to be tested in future studies. It is also possible that trypanosomatid-specific subunits could be assembled as a jigsaw puzzle-like membrane anchor.

*Spectroscopic Properties of T. cruzi Complex II*—Pyridine ferrohemochrome analysis showed that *T. cruzi* Complex II binds a stoichiometric amount of protoheme IX (0.85 heme/monomer of enzyme) indicating that monomer enzyme complex contains one heme. At room temperature, the air-oxidized and fully reduced forms of the purified enzyme showed peaks at 413 and 426, 527, and 561 nm, respectively (Fig. 6). Peak positions are similar to those reported for Complex II from *E. coli* (40), adult *A. suum* (41), and bovine (42, 43), where heme is ligated via histidine in the second helices of SDH3 and SDH4. Although heme has an important role in the assembly of Complex II, it is not essential for the reduction of ubiquinones (43, 44).

*Enzymatic Properties of T. cruzi Complex II*—We examined SQR activity of the purified enzyme and found the difference in apparent $K_m$ values between $Q_1$ (33.9 ± 3.6 μM) and $Q_2$ (18.8 ± 6.4 μM) (Fig. 7), indicating that the 6-polyprenyl group of ubiquinone contributes to the binding affinity. The apparent $V_{max}$ value of the *T. cruzi* Complex II was rather constant, 11.9 ± 2.2 for $Q_1$ and 11.5 ± 0.4 $Q_2$ units/mg proteins, respectively, and one-fourth of those reported for bovine and *E. coli* enzymes (45, 46). This is not surprising because *T. cruzi* complex II has about 2–3 times more proteins than the other enzymes. $K_m$ values for ubiquinone and succinate (18.8 ± 6.4 μM ($Q_2$) and 1.48 ± 0.17 mM, respectively) were higher than 0.3 and 130 μM, respectively, of bovine enzyme (45), and 2 and 277 μM, respectively, of the *E. coli* enzyme (46, 47). Notably, the $K_m$ value for succinate was comparable with 610 μM in adult *A. suum* (10), which expresses the stage-specific Complex II as quinol:fumarate reductase under hypoxic habitats in host organisms.

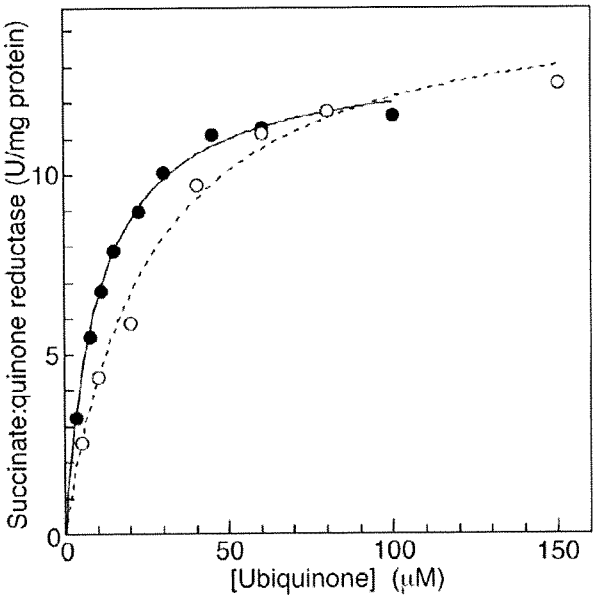


FIGURE 7. **Kinetic analysis of succinate-quinone reductase activity.** Succinate:ubiquinone reductase activity of the purified Complex II was determined with $Q_1$ (○) and $Q_2$ (●) at a protein concentration of 1.25 μg/ml in the presence of 10 mM sodium succinate. Data were fitted with the Michaelis-Menten equation using KaleidaGraph, and apparent $K_m$ and $V_{max}$ values were 30.3 ± 4.3 μM and 14.0 ± 1.2 units/mg protein, respectively, for $Q_1$ and 12.4 ± 0.7 μM and 11.9 ± 0.3 units/mg protein, respectively, for $Q_2$.

Then we examined effects of inhibitors for binding sites of quinones and dicarboxylates on SQR activity. Atpenin A5, a potent inhibitor for Complex II, inhibited the *T. cruzi* enzyme with the $IC_{50}$ value of 6.4 ± 2.4 μM, which is 3 orders of magnitude higher than that of bovine Complex II (4 nM) (48). Furthermore, carboxin, 2-theonyltrifluoroacetone, plumbagin, and 2-heptyl-4-hydroxyquinoline *N*-oxide were ineffective (100 μM $<IC_{50}$). Structural divergence in trypanosomatid SDH3 and SDH4 could be the cause for lower binding affinities for both quinones and inhibitors. In addition, we found for the dicarboxylate-binding site that the $IC_{50}$ value for malonate (40 μM) was much higher than the $K_i$ value for bovine Complex II (1.3 μM) (45).

*Structure of Trypanosomatid Complex II*—To the best of our knowledge, this is the first report on the isolation of protist Complex II. *T. cruzi* Complex II has unusual subunit organization with six each of hydrophilic and hydrophobic subunits. Such a supramolecular structure and heterodimeric SDH2 ($SDH2_N$ and $SDH2_C$) are conserved in the Trypanosomatida. Furthermore, SDH1, $SDH2_N$, $SDH2_C$, SDH3, SDH4, and SDH8–SDH10 can be identified in the ongoing genome projects on the evolutionary relatives, the photosynthetic free-living *Euglena gracilis*, and the nonphotosynthetic euglenoid *Astasia longa* in the Euglenida. Thus a part of these features are common in the Euglenozoa, a divergent lineage of eukaryotes (Fig. 8).

Accumulation of noncatalytic subunits through expanding the protein interaction network could be a driving force for protein evolution. Structural and catalytic features are unique, and thus this enzyme could be a potential target for novel chemotherapeutic agents for trypanosomiasis and leishmaniasis.

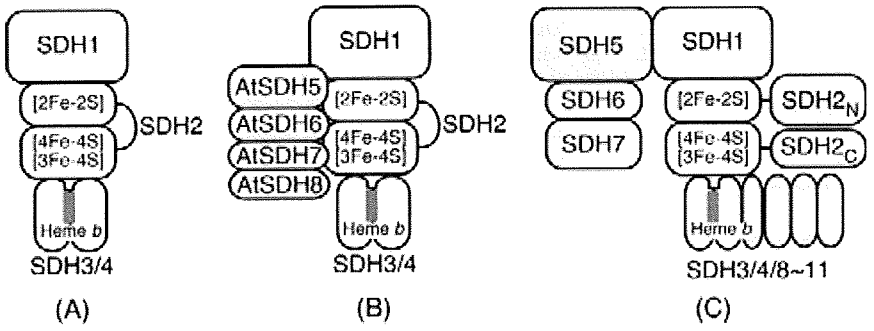


FIGURE 8. **Subunit organization of Complex II.** *A*, common four-subunit Complex II (*e.g.* mammals, *E. coli*); *B*, eight-subunit Complex II in plants (*e.g. A. thaliana*); and *C*, 12-subunit Complex II in the Trypanosomatida. Noncatalytic subunits and domains are shown in *yellow* and heme in *red*.

*Conclusion*—The parasitic protist *T. brucei* is a gold mine where unprecedented biological phenomena like RNA editing and trans-splicing in mitochondria were originally discovered. It was found recently in *Diplonema papillatum*, a free-living evolutionary cousin,

that mature mRNA for cytochrome *c* oxidase CoxI was assembled from nine gene fragments by a jigsaw puzzle mechanism (49). From a characterization of Complex II from *T. cruzi*, we revealed a novel supramolecular organization, which is conserved in the Trypanosomatida.

Parasites have exploited unique energy metabolic pathways as adaptations to their natural habitats within their hosts (50, 51). In fact, the respiratory systems of parasites typically show greater diversity in electron transfer pathways than those of host animals. As shown in this study, such is also the case with Complex II, which is a well known marker enzyme of mitochondria. Studies on the role of supramolecular Complex II in adaptation of trypanosomatids is now underway in our laboratory.

*Acknowledgments—We thank Drs. J. L. Concepcion (Universidad de Los Andes, Merida-Venezuela) and T. Nara (Juntendo University) for kind advice; and Drs. M. Matsuzaki (University of Tokyo), T. Hashimoto (University of Tsukuba), G. Cecchini (University of California San Francisco), and M. Müller (Rockefeller University) for critical reading of the manuscript.*

## REFERENCES

1. World Health Organization (2007) *Report of the First Meeting of WHO Strategic and Technical Advisory Group on Neglected Tropical Diseases,* pp. 1–26, Geneva, Switzerland
2. Berriman, M., Ghedin, E., Hertz-Fowler, C., Blandin, G., Renauld, H., Bartholomeu, D. C., Lennard, N. J., Caler, E., Hamlin, N. E., Haas, B., Bohme, U., Hannick, L., Aslett, M. A., Shallom, J., Marcello, L., Hou, L., Wickstead, B., Alsmark, U. C., Arrowsmith, C., Atkin, R. J., Barron, A. J., Bringaud, F., Brooks, K., Carrington, M., Cherevach, I., Chillingworth, T. J., Churcher, C., Clark, L. N., Corton, C. H., Cronin, A., Davies, R. M., Doggett, J., Djikeng, A., Feldblyum, T., Field, M. C., Fraser, A., Goodhead, I., Hance, Z., Harper, D., Harris, B. R., Hauser, H., Hostetler, J., Ivens, A., Jagels, K., Johnson, D., Johnson, J., Jones, K., Kerhornou, A. X., Koo, H., Larke, N., Landfear, S., Larkin, C., Leech, V., Line, A., Lord, A., Macleod, A., Mooney, P. J., Moule, S., Martin, D. M., Morgan, G. W., Mungall, K., Norbertczak, H., Ormond, D., Pai, G., Peacock, C. S., Peterson, J., Quail, M. A., Rabbinowitsch, E., Rajandream, M. A., Reitter, C., Salzberg, S. L., Sanders, M., Schobel, S., Sharp, S., Simmonds, M., Simpson, A. J., Tallon, L., Turner, C. M., Tait, A., Tivey, A. R., Van Aken, S., Walker, D., Wanless, D., Wang, S., White, B., White, O., Whitehead, S., Woodward, J., Wortman, J., Adams, M. D., Embley, T. M., Gull, K., Ullu, E., Barry, J. D., Fairlamb, A. H., Opperdoes, F., Barrell, B. G., Donelson, J. E., Hall, N., Fraser, C. M., Melville, S. E., and El-Sayed, N. M. (2005) *Science* **309,** 416–422
3. Cazzulo, J. J. (1994) *J. Bioenerg. Biomembr.* **26,** 157–165
4. Besteiro, S., Barrett, M. P., Riviere, L., and Bringaud, F. (2005) *Trends Parasitol.* **21,** 185–191
5. Bringaud, F., Riviere, L., and Coustou, V. (2006) *Mol. Biochem. Parasitol.* **149,** 1–9
6. Takashima, E., Inaoka, D. K., Osanai, A., Nara, T., Odaka, M., Aoki, T., Inaka, K., Harada, S., and Kita, K. (2002) *Mol. Biochem. Parasitol.* **122,** 189–200
7. Van Hellemond, J. J., Opperdoes, F. R., and Tielens, A. G. (1998) *Proc. Natl. Acad. Sci. U. S. A.* **95,** 3036–3041
8. Harington, J. S. (1961) *Parasitology* **51,** 309–318
9. Roos, M. H., and Tielens, A. G. (1994) *Mol. Biochem. Parasitol.* **66,** 273–281
10. Saruta, F., Kuramochi, T., Nakamura, K., Takamiya, S., Yu, Y., Aoki, T., Sekimizu, K., Kojima, S., and Kita, K. (1995) *J. Biol. Chem.* **270,** 928–932
11. Cecchini, G. (2003) *Annu. Rev. Biochem.* **72,** 77–109
12. Yankovskaya, V., Horsefield, R., Tornroth, S., Luna-Chavez, C., Miyoshi, H., Leger, C., Byrne, B., Cecchini, G., and Iwata, S. (2003) *Science* **299,** 700–704
13. Sun, F., Huo, X., Zhai, Y., Wang, A., Xu, J., Su, D., Bartlam, M., and Rao, Z. (2005) *Cell* **121,** 1043–1057
14. Huang, L. S., Sun, G., Cobessi, D., Wang, A. C., Shen, J. T., Tung, E. Y., Anderson, V. E., and Berry, E. A. (2006) *J. Biol. Chem.* **281,** 5965–5972
15. El-Sayed, N. M., Myler, P. J., Bartholomeu, D. C., Nilsson, D., Aggarwal, G., Tran, A. N., Ghedin, E., Worthey, E. A., Delcher, A. L., Blandin, G., Westenberger, S. J., Caler, E., Cerqueira, G. C., Branche, C., Haas, B., Anupama, A., Arner, E., Aslund, L., Attipoe, P., Bontempi, E., Bringaud, F., Burton, P., Cadag, E., Campbell, D. A., Carrington, M., Crabtree, J., Darban, H., da Silveira, J. F., de Jong, P., Edwards, K., Englund, P. T., Fazelina, G., Feldblyum, T., Ferella, M., Frasch, A. C., Gull, K., Horn, D., Hou, L., Huang, Y., Kindlund, E., Klingbeil, M., Kluge, S., Koo, H., Lacerda, D., Levin, M. J., Lorenzi, H., Louie, T., Machado, C. R., McCulloch, R., McKenna, A., Mizuno, Y., Mottram, J. C., Nelson, S., Ochaya, S., Osoegawa, K., Pai, G., Parsons, M., Pentony, M., Pettersson, U., Pop, M., Ramirez, J. L., Rinta, J., Robertson, L., Salzberg, S. L., Sanchez, D. O., Seyler, A., Sharma, R., Shetty, J., Simpson, A. J., Sisk, E., Tammi, M. T., Tarleton, R., Teixeira, S., Van Aken, S., Vogt, C., Ward, P. N., Wickstead, B., Wortman, J., White, O., Fraser, C. M., Stuart, K. D., and Andersson, B. (2005) *Science* **309,** 409–415
16. Ivens, A. C., Peacock, C. S., Worthey, E. A., Murphy, L., Aggarwal, G., Berriman, M., Sisk, E., Rajandream, M. A., Adlem, E., Aert, R., Anupama, A., Apostolou, Z., Attipoe, P., Bason, N., Bauser, C., Beck, A., Beverley, S. M., Bianchettin, G., Borzym, K., Bothe, G., Bruschi, C. V., Collins, M., Cadag, E., Ciarloni, L., Clayton, C., Coulson, R. M., Cronin, A., Cruz, A. K., Davies, R. M., De Gaudenzi, J., Dobson, D. E., Duesterhoeft, A., Fazelina, G., Fosker, N., Frasch, A. C., Fraser, A., Fuchs, M., Gabel, C., Goble, A., Goffeau, A., Harris, D., Hertz-Fowler, C., Hilbert, H., Horn, D., Huang, Y., Klages, S., Knights, A., Kube, M., Larke, N., Litvin, L., Lord, A., Louie, T., Marra, M., Masuy, D., Matthews, K., Michaeli, S., Mottram, J. C., Muller-Auer, S., Munden, H., Nelson, S., Norbertczak, H., Oliver, K., O'Neil, S., Pentony, M., Pohl, T. M., Price, C., Purnelle, B., Quail, M. A., Rabbinowitsch, E., Reinhardt, R., Rieger, M., Rinta, J., Robben, J., Robertson, L., Ruiz, J. C., Rutter, S., Saunders, D., Schafer, M., Schein, J., Schwartz, D. C., Seeger, K., Seyler, A., Sharp, S., Shin, H., Sivam, D., Squares, R., Squares, S., Tosato, V., Vogt, C., Volckaert, G., Wambutt, R., Warren, T., Wedler, H., Woodward, J., Zhou, S., Zimmermann, W., Smith, D. F., Blackwell, J. M., Stuart, K. D., Barrell, B., and Myler, P. J. (2005) *Science* **309,** 436–442
17. Bourguignon, S. C., Mello, C. B., Santos, D. O., Gonzalez, M. S., and Souto-Padron, T. (2006) *Acta Trop.* **98,** 103–109
18. Concepcion, J. L., Chataing, B., and Dubourdieu, M. (1999) *Comp. Biochem. Physiol.* **122,** 211–222
19. Matsudaira, P. (1987) *J. Biol. Chem.* **262,** 10035–10038
20. Rosenfeld, J., Capdevielle, J., Guillemot, J. C., and Ferrara, P. (1992) *Anal. Biochem.* **203,** 173–179
21. Brusca, J. S., and Radolf, J. D. (1994) *Methods Enzymol.* **228,** 182–193
22. Wittig, I., Karas, M., and Schagger, H. (2007) *Mol. Cell. Proteomics* **6,** 1215–1225
23. Sabar, M., Balk, J., and Leaver, C. J. (2005) *Plant J.* **44,** 893–901
24. Berry, E. A., and Trumpower, B. L. (1987) *Anal. Biochem.* **161,** 1–15
25. Larkin, M. A., Blackshields, G., Brown, N. P., Chenna, R., McGettigan, P. A., McWilliam, H., Valentin, F., Wallace, I. M., Wilm, A., Lopez, R., Thompson, J. D., Gibson, T. J., and Higgins, D. G. (2007) *Bioinformatics (Oxf.)* **23,** 2947–2948
26. Schagger, H., and Pfeiffer, K. (2000) *EMBO J.* **19,** 1777–1783
27. Millar, A. H., Eubel, H., Jansch, L., Kruft, V., Heazlewood, J. L., and Braun, H. P. (2004) *Plant Mol. Biol.* **56,** 77–90
28. Eubel, H., Heinemeyer, J., and Braun, H. P. (2004) *Plant Physiol.* **134,** 1450–1459
29. Eubel, H., Heinemeyer, J., Sunderhaus, S., and Braun, H. P. (2004) *Plant Physiol. Biochem.* **42,** 937–942
30. Horsefield, R., Yankovskaya, V., Sexton, G., Whittingham, W., Shiomi, K., Omura, S., Byrne, B., Cecchini, G., and Iwata, S. (2006) *J. Biol. Chem.* **281,** 7309–7316
31. Allen, J. W., Ginger, M. L., and Ferguson, S. J. (2004) *Biochem. J.* **383,** 537–542
32. Funes, S., Davidson, E., Reyes-Prieto, A., Magallon, S., Herion, P., King, M. P., and Gonzalez-Halphen, D. (2002) *Science* **298,** 2155

33. Waller, R. F., and Keeling, P. J. (2006) *Gene (Amst.)* **383,** 33–37
34. Williams, N., and Frank, P. H. (1990) *Mol. Biochem. Parasitol.* **43,** 125–132
35. Nelson, R. E., Aphasizheva, I., Falick, A. M., Nebohacova, M., and Simpson, L. (2004) *Mol. Biochem. Parasitol.* **135,** 221–224
36. Adams, K. L., Rosenblueth, M., Qiu, Y. L., and Palmer, J. D. (2001) *Genetics* **158,** 1289–1300
37. Tran, Q. M., Rothery, R. A., Maklashina, E., Cecchini, G., and Weiner, J. H. (2006) *J. Biol. Chem.* **281,** 32310–32317
38. Yang, X., Yu, L., He, D., and Yu, C. A. (1998) *J. Biol. Chem.* **273,** 31916–31923
39. Maklashina, E., Rothery, R. A., Weiner, J. H., and Cecchini, G. (2001) *J. Biol. Chem.* **276,** 18968–18976
40. Kita, K., Vibat, C. R., Meinhardt, S., Guest, J. R., and Gennis, R. B. (1989) *J. Biol. Chem.* **264,** 2672–2677
41. Takamiya, S., Furushima, R., and Oya, H. (1986) *Biochim. Biophys. Acta* **848,** 99–107
42. Tushurashvili, P. R., Gavrikova, E. V., Ledenev, A. N., and Vinogradov, A. D. (1985) *Biochim. Biophys. Acta* **809,** 145–159
43. Tran, Q. M., Rothery, R. A., Maklashina, E., Cecchini, G., and Weiner, J. H. (2007) *Proc. Natl. Acad. Sci. U. S. A.* **104,** 18007–18012
44. Oyedotun, K. S., Sit, C. S., and Lemire, B. D. (2007) *Biochim. Biophys. Acta* **1767,** 1436–1445
45. Grivennikova, V. G., Gavrikova, E. V., Timoshin, A. A., and Vinogradov, A. D. (1993) *Biochim. Biophys. Acta* **1140,** 282–292
46. Maklashina, E., and Cecchini, G. (1999) *Arch. Biochem. Biophys.* **369,** 223–232
47. Miyadera, H., Hiraishi, A., Miyoshi, H., Sakamoto, K., Mineki, R., Murayama, K., Nagashima, K. V., Matsuura, K., Kojima, S., and Kita, K. (2003) *Eur. J. Biochem.* **270,** 1863–1874
48. Miyadera, H., Shiomi, K., Ui, H., Yamaguchi, Y., Masuma, R., Tomoda, H., Miyoshi, H., Osanai, A., Kita, K., and Omura, S. (2003) *Proc. Natl. Acad. Sci. U. S. A.* **100,** 473–477
49. Marande, W., and Burger, G. (2007) *Science* **318,** 415
50. Kita, K., and Takamiya, S. (2002) *Adv. Parasitol.* **51,** 95–131
51. Tielens, A. G., Rotte, C., van Hellemond, J. J., and Martin, W. (2002) *Trends Biochem. Sci.* **27,** 564–572
52. Krogh, A., Larsson, B., von Heijne, G., and Sonnhammer, E. L. L. (2001) *J. Mol. Biol.* **305,** 567–580
53. Mitaku, S., Hirokawa, T., and Tsuji, T. (2002) *Bioinformatics* **18,** 608–616

Cell Metabolism
Article

# Fasting-Induced Hypothermia and Reduced Energy Production in Mice Lacking Acetyl-CoA Synthetase 2

Iori Sakakibara,[1,2] Takahiro Fujino,[3] Makoto Ishii,[2,4] Toshiya Tanaka,[1] Tatsuo Shimosawa,[5] Shinji Miura,[6] Wei Zhang,[7] Yuka Tokutake,[8] Joji Yamamoto,[2,9] Mutsumi Awano,[10] Satoshi Iwasaki,[1,2] Toshiyuki Motoike,[2,11] Masashi Okamura,[1,9] Takeshi Inagaki,[1] Kiyoshi Kita,[10] Osamu Ezaki,[6] Makoto Naito,[13] Tomoyuki Kuwaki,[7] Shigeru Chohnan,[8] Tokuo T. Yamamoto,[14] Robert E. Hammer,[12] Tatsuhiko Kodama,[1] Masashi Yanagisawa,[2,11] and Juro Sakai[1,2,*]

[1]Laboratory for Systems Biology and Medicine, Research Center for Advanced Science and Technology, University of Tokyo, Tokyo 153-8904, Japan

[2]ERATO, Japan Science and Technology Agency (JST), Tokyo 102-0075, Japan

[3]Department of Bioscience, Integrated Center for Sciences, Ehime University Graduate School of Medicine, Ehime 791-0295, Japan

[4]Department of Neurology, Weill Cornell Medical College of Cornell University, 525 East 68th Street, New York, NY 10021, USA

[5]Department of Clinical Laboratory, Faculty of Medicine, University of Tokyo, Tokyo 113-8655, Japan

[6]Nutritional Science Program, National Institute of Health and Nutrition, 1-23-1, Toyama, Shinjuku-ku, Tokyo 162-8636, Japan

[7]Departments of Molecular & Integrative Physiology and Autonomic Physiology, Graduate School of Medicine, Chiba University, Chiba, 260-8670, Japan

[8]Department of Bioresource Science, Ibaraki University College of Agriculture, 3-21-1 Chuo, Ami, Ibaraki 300-0393, Japan

[9]Division of Nephrology, Endocrinology, and Vascular Medicine, Department of Medicine, Tohoku University Graduate School of Medicine, Sendai 980-8574, Japan

[10]Department of Biomedical Chemistry, Graduate School of Medicine, University of Tokyo, Bunkyo-ku, Tokyo 113-0033, Japan

[11]Howard Hughes Medical Institute, Department of Molecular Genetics

[12]Department of Biochemistry
University of Texas Southwestern Medical Center, Dallas, TX 75390, USA

[13]Department of Cellular Function, Division of Cellular and Molecular Pathology, Niigata University Graduate School of Medical and Dental Sciences, Niigata 951-8510, Japan

[14]Center for Advanced Genome Research, Institute of Development, Aging, and Cancer, Tohoku University, Sendai 981-8555, Japan

*Correspondence: jmsakai-tky@umin.ac.jp

DOI 10.1016/j.cmet.2008.12.008

## SUMMARY

Acetate is activated to acetyl-CoA by acetyl-CoA synthetase 2 (AceCS2), a mitochondrial enzyme. Here, we report that the activation of acetate by AceCS2 has a specific and unique role in thermogenesis during fasting. In the skeletal muscle of fasted *AceCS2*$^{-/-}$ mice, ATP levels were reduced by 50% compared to *AceCS2*$^{+/+}$ mice. Fasted *AceCS2*$^{-/-}$ mice were significantly hypothermic and had reduced exercise capacity. Furthermore, when fed a low-carbohydrate diet, 4-week-old weaned *AceCS2*$^{-/-}$ mice also exhibited hypothermia accompanied by sustained hypoglycemia that led to a 50% mortality. Therefore, AceCS2 plays a significant role in acetate oxidation needed to generate ATP and heat. Furthermore, *AceCS2*$^{-/-}$ mice exhibited increased oxygen consumption and reduced weight gain on a low-carbohydrate diet. Our findings demonstrate that activation of acetate by AceCS2 plays a pivotal role in thermogenesis, especially under low-glucose or ketogenic conditions, and is crucially required for survival.

## INTRODUCTION

Mammals have evolved complex metabolic systems to survive extended periods of nutrient deprivation. Under a fed condition, mammals utilize glucose as the main metabolic fuel. Under ketogenic conditions such as fasting, low-carbohydrate diet feeding, and diabetes, fatty acids and ketone bodies are utilized as the main energy sources. Ketone bodies, utilized mainly in brain and also some in skeletal muscle and heart (Fukao et al., 2004), are produced in liver from acetyl-CoA released after β oxidation of fatty acids in mitochondria. Several lines of evidence report that acetate is synthesized in the liver and utilized as an alternative fuel under ketogenic conditions. For instance, acetate concentration in livers of starved rats is quite high (Murthy and Steiner, 1973). Also, formation of free acetate by the liver has been reported from studies utilizing isolated rat liver perfusion and studies using isolated hepatocytes (Leighton et al., 1989; Seufert et al., 1974; Yamashita et al., 2001). Acetate is generated following hydrolysis of acetyl-CoA by acetyl CoA hydrolase, an end product of fatty acid oxidation in rat liver peroxisomes (Leighton et al., 1989). However, it is not known whether acetate is actually utilized as an alternative fuel (substituting for glucose, fatty acids, or ketone bodies) in peripheral tissues such as skeletal muscle, heart, brown adipose tissues (BAT), or brain.

Acetyl-CoA synthetase (AceCS, EC 6.2.1.1) ligates acetate and CoA to generate acetyl-CoA. In mammals, there are two AceCSs with similar enzymatic properties: one, designated AceCS1, is a cytosolic enzyme, whereas AceCS2 is an enzyme of the mitochondrial matrix (Fujino et al., 2001; Luong et al., 2000). AceCS1 and AceCS2 are regulated posttranscriptionally by members of the sirtuin family of deacetylases, SIRT1 and SIRT3, respectively. Both SIRT1 and SIRT3 are upregulated during caloric restriction and have been implicated as mediating

the longevity-promoting effects of caloric restriction (Schwer and Verdin, 2008; Yang et al., 2007).

AceCS1 provides acetyl-CoA for the synthesis of fatty acids and cholesterol. AceCS1 is highly expressed in liver, and its transcription is regulated by sterol regulatory element-binding proteins (SREBPs), basic helix-loop-helix leucine zipper transcription factors that activate multiple genes involved in cholesterol and fatty acid metabolism (Ikeda et al., 2001; Luong et al., 2000). By contrast, AceCS2 produces acetyl-CoA for oxidation through the tricarboxylic acid cycle to produce ATP and $CO_2$ (Fujino et al., 2001). AceCS2 is highly expressed in BAT, heart, and skeletal muscle. Importantly, the levels of its mRNAs in BAT, heart, and skeletal muscle are robustly increased under ketogenic conditions, whereas the level of its mRNAs in liver was barely detectable (Fujino et al., 2001). The fasting-induced transcriptional activation of AceCS2 in the skeletal muscle is largely controlled by Krüppel-like factor 15 (KLF15), a member of the Krüppel-like family of transcription factors (Yamamoto et al., 2004) that regulates many genes involved in gluconeogenesis such as phosphoenolpyruvate carboxykinase (PEPCK) and amino acid-degrading enzymes required under ketogenic conditions (Gray et al., 2007; Teshigawara et al., 2005).

To examine whether acetate is utilized as a fuel under ketogenic conditions, we generated *AceCS2*-deficient mice. In this paper, we show that AceCS2 is essential for energy expenditure under ketogenic conditions.

## RESULTS

### Generation of *AceCS2*-Deficient Mice

To evaluate the role of AceCS2 in vivo, we generated mice lacking *AceCS2*. We constructed an insertion-type vector that disrupts exon 1 of the mouse *AceCS2* gene (Figure 1A). Two lines of mice harboring insertions in *AceCS2* were identified by Southern blotting (Figure 1B). Genotyping was performed by PCR (Figure 1C), and the absence of AceCS2 transcripts (Figure 1D) and protein (Figure 1E) was confirmed by quantitative real-time PCR (QRT-PCR) and immunoblot analysis, respectively. Wild-type (*AceCS2*$^{+/+}$), heterozygous (*AceCS2*$^{+/-}$), and homozygous (*AceCS2*$^{-/-}$) mice were born at frequencies predicted by simple Mendelian ratios. *AceCS2*$^{-/-}$ mice of both sexes were normally fertile and typical in appearance. No histological abnormalities were seen following light microscopy of sections obtained from multiple tissues of adult male mice, including bone, brain, stomach, heart, intestine, kidney, liver, pancreas, white adipose tissue, BAT, and skeletal muscle (data not shown). At birth, the body weight and length of *AceCS2*$^{-/-}$ mice were indistinguishable from their littermates. By the time of weaning (4 weeks of age), both male and female *AceCS2*$^{-/-}$ mice exhibited significant growth retardation (Figures S1A–S1C available online). After weaning, *AceCS2*$^{-/-}$ mice fed on normal chow diet began to catch up with *AceCS2*$^{+/+}$ mice in both body weight and body length. By 20 weeks of age, the body weight of the *AceCS2*$^{-/-}$ mice became comparable to their littermates (Figures S1A and S1B). Food intake of 4-week-old *AceCS2*$^{-/-}$ mice was slightly decreased compared to *AceCS2*$^{+/+}$ mice but became comparable to that of their littermates by 20 weeks of age (Figure S1D). Plasma parameters of *AceCS2*$^{+/+}$ and *AceCS2*$^{-/-}$ mice before weaning

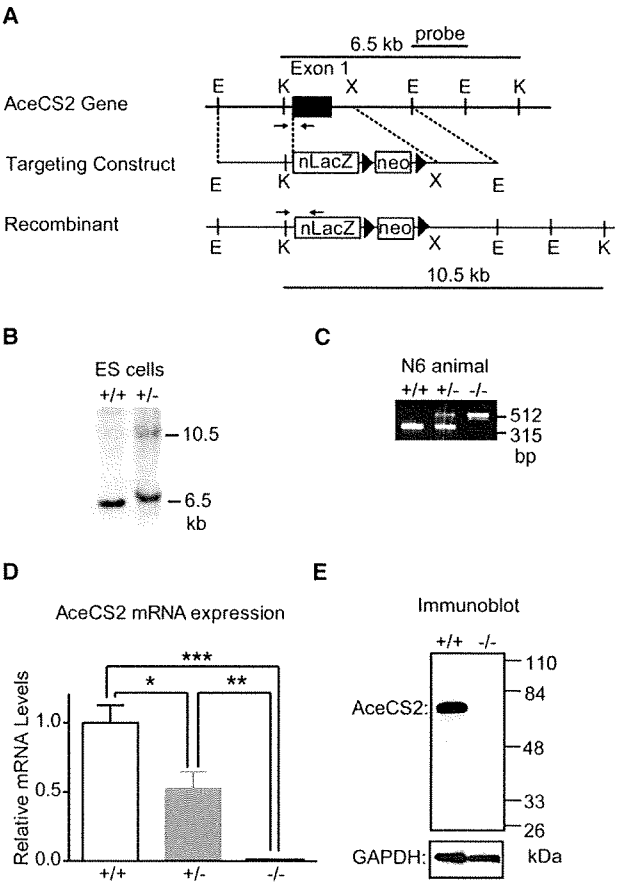


**Figure 1. Generation of *AceCS2*-Deficient Mice**

(A) Diagram of the targeting strategy. Only the relevant restriction sites are indicated. Locations of the probes for Southern blot analysis (bars) and PCR primers (arrows) for genotyping are shown.

(B) Southern blot analysis of KpnI-digested DNA from ES cell clones. Southern blotting was performed with the probe indicated in (A). KpnI digestion resulted in a 6.5 kb fragment in wild-type DNA and a 10.5 kb fragment in homologous recombinants.

(C) An ethidium bromide-stained agarose gel illustrates PCR products for genotyping *AceCS2*$^{+/+}$, *AceCS2*$^{+/-}$, and *AceCS2*$^{-/-}$ mice. A description of the PCR genotyping strategy is contained in the Experimental Procedures.

(D) QRT-PCR analysis of AceCS2 transcripts. Total RNA from heart of *AceCS2*$^{+/+}$, *AceCS2*$^{+/-}$, and *AceCS2*$^{-/-}$ mice were analyzed by QRT-PCR quantification as described in the Experimental Procedures. β-actin was used as the invariant control. Values represent the amount of mRNA relative to that in *AceCS2*$^{+/+}$ mice, which is arbitrarily defined as 1. Data are mean ± SEM. *$p < 0.05$ compared to *AceCS2*$^{+/+}$; **$p < 0.01$ compared to *AceCS2*$^{+/-}$; ***$p < 0.001$ compared to *AceCS2*$^{+/+}$ ($^{+/+}$, n = 9; $^{+/-}$, n = 17; $^{-/-}$, n = 7).

(E) Immunoblot analysis, with an affinity-purified anti-rabbit polyclonal AceCS2 antibody, of *AceCS2*$^{+/+}$ and *AceCS2*$^{-/-}$ mouse heart protein. Each lane was loaded with 20 μg of whole-cell lysates in SDS lysis buffer from the hearts. GAPDH was detected with a polyclonal anti-GAPDH antibody as a loading control.

(2–4 weeks of age) and at 26 weeks of age are shown in Table S1. Glucose, ketone bodies, nonesterified fatty acids (NEFA), and insulin levels were indistinguishable between *AceCS2*$^{+/+}$ and *AceCS2*$^{-/-}$ mice at both 2–4 weeks of age and at 26 weeks of age (Table S1). Plasma concentration of growth hormone and

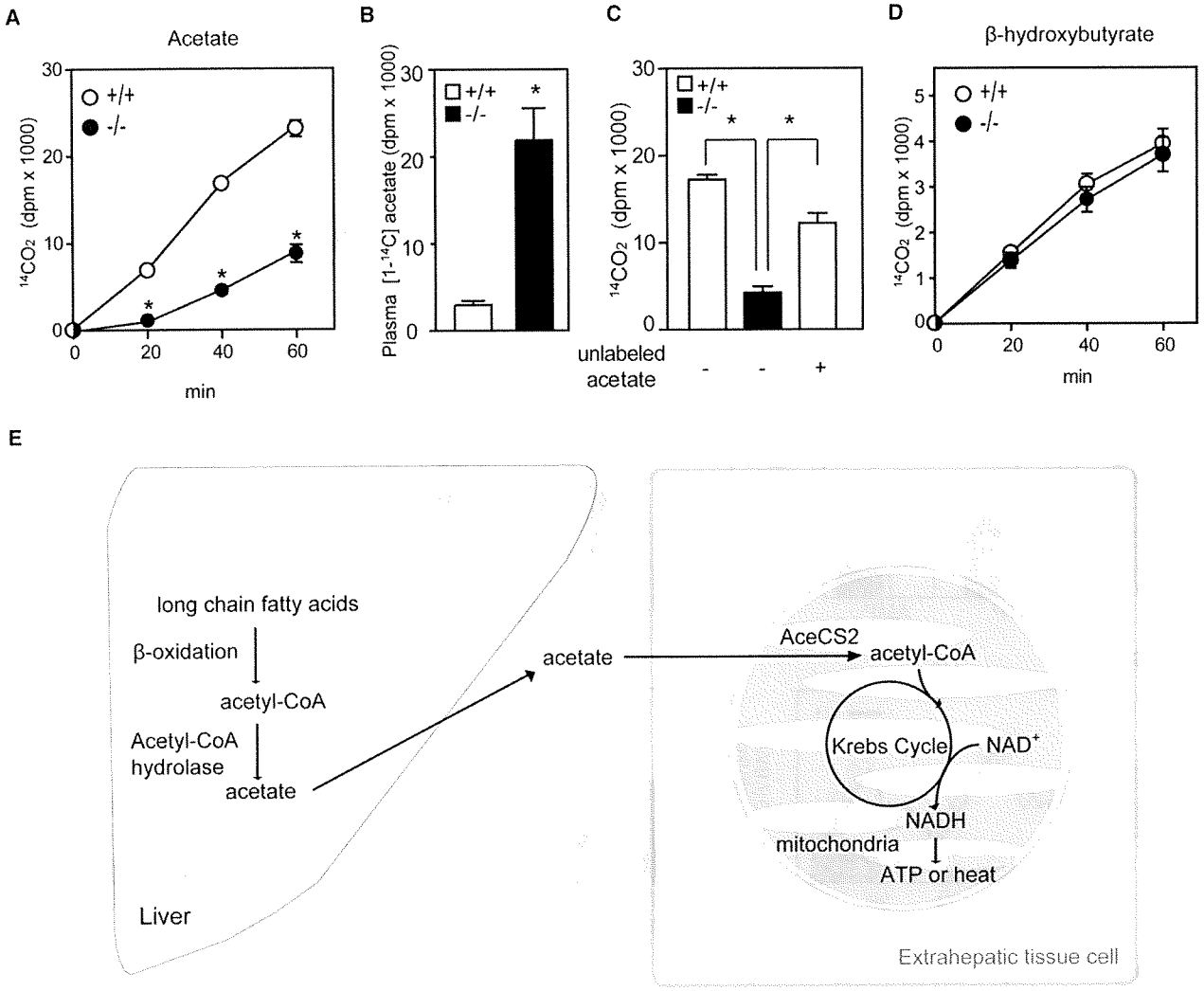


Figure 2. *AceCS2*$^{-/-}$ Mice Exhibit Lower Whole-Body Acetic Acid Oxidation during Fasting

After 48 hr of fasting, 12-week-old male mice were tested for their ability to oxidize [1-$^{14}$C]acetate or [1-$^{14}$C]β-hydroxybutyrate to $^{14}CO_2$ at 20, 40, and 60 min after intraperitoneal (i.p.) injection with the labeled compound.

(A) Rate of $^{14}CO_2$ production from acetate. *$p < 0.001$ compared to *AceCS2*$^{+/+}$.

(B) Total plasma [1-$^{14}$C]acetate was measured after 60 min.

(C) Rate of $^{14}CO_2$ production from acetate with inclusion of unlabeled acetate. Unlabeled acetate (0.6 g/kg) was injected with [1-$^{14}$C]acetate, and the acetate oxidation rate was measured after 40 min.

(D) Rate of $^{14}CO_2$ production from β-hydroxybutyrate (*AceCS2*$^{+/+}$, n = 6; *AceCS2*$^{-/-}$, n = 6).

(E) Model for the role of AceCS2 in energy metabolism.

(A–D) Data are mean ± SEM.

insulin-like growth factor-1 (IGF-1) of *AceCS2*$^{-/-}$ mice (2–4 weeks of age) were also comparable to *AceCS2*$^{+/+}$. The plasma leptin levels of 2- to 4-week-old *AceCS2*$^{-/-}$ mice were lower than those of age-matched, wild-type littermates. Notably, plasma acetate levels were markedly elevated in *AceCS2*$^{-/-}$ mice compared to *AceCS2*$^{+/+}$ mice (Table S1).

### *AceCS2*$^{-/-}$ Mice Exhibited Marked Reduction in Whole-Body Acetate Oxidation

To examine whether acetate is, in fact, utilized as a fuel during fasting, we performed whole-body acetate oxidization assays. Mice were fasted for 48 hr and then injected with [$^{14}$C]acetate. Figure 2A shows the sharply decreased rate of acetate oxidation in *AceCS2*$^{-/-}$ mice. As a consequence, [$^{14}$C]acetate levels remained high in the plasma of *AceCS2*$^{-/-}$ mice, whereas *AceCS2*$^{+/+}$ mice showed very low levels of plasma [$^{14}$C]acetate (Figure 2B). Because higher levels of plasma acetate in *AceCS2*$^{-/-}$ mice might affect the acetate oxidation rate, we also examined the oxidation of [$^{14}$C]acetate with the inclusion of unlabeled acetate at similar levels to those found in the *AceCS2*$^{-/-}$ mice (about 2 mM) (Figure 2C). Injection of unlabeled acetate (0.6 mg/kg) led to rapid increase in plasma acetate to

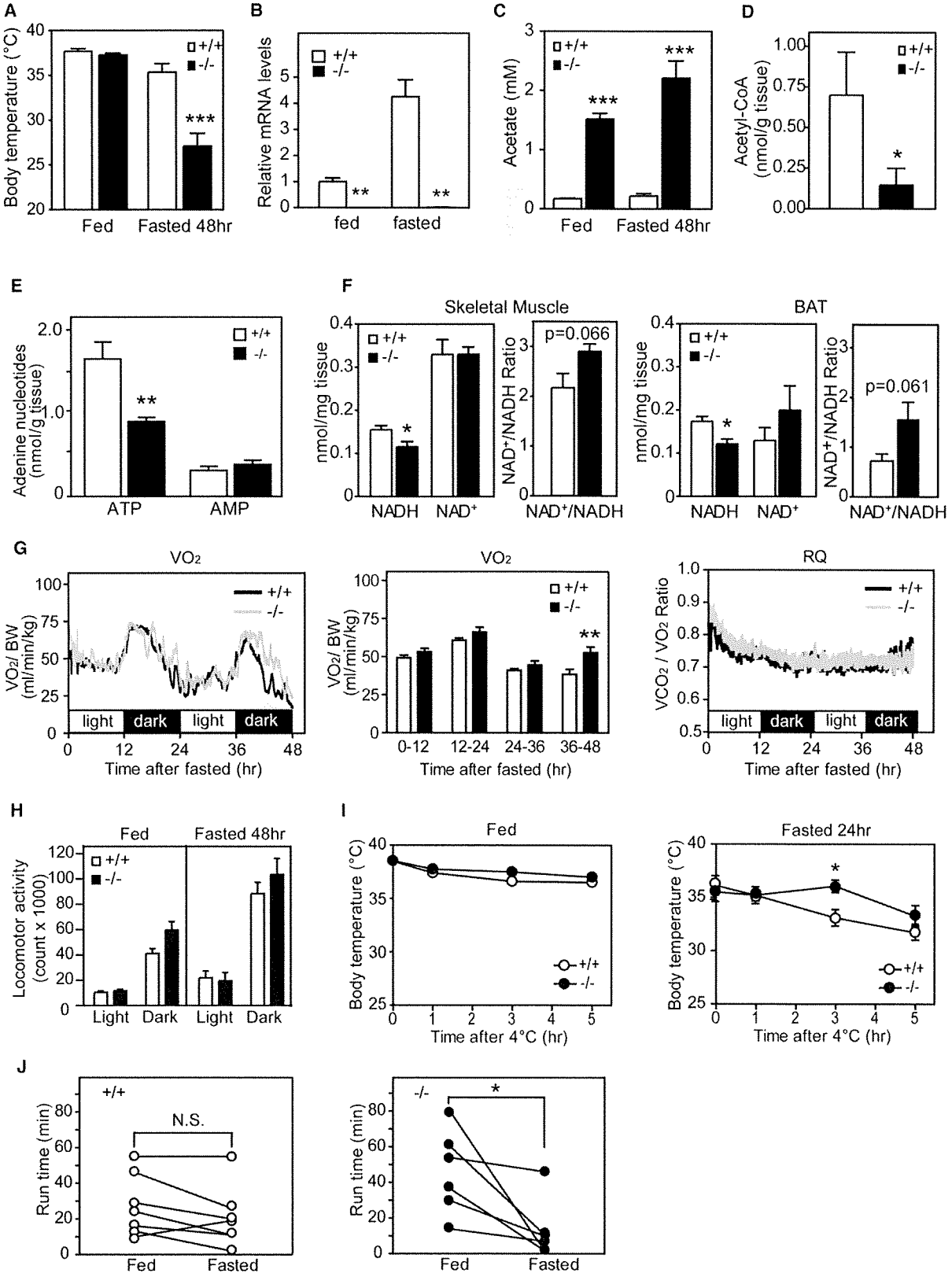
A
Body temperature (°C)
+/+
-/-
***
Fed
Fasted 48hr
B
Relative mRNA levels
+/+
-/-
**
**
fed
fasted
C
Acetate (mM)
+/+
-/-
***
***
Fed
Fasted 48hr
D
Acetyl-CoA (nmol/g tissue)
+/+
-/-
*
E
Adenine nucleotides (nmol/g tissue)
+/+
-/-
**
ATP
AMP
F
Skeletal Muscle
BAT
nmol/mg tissue
NAD+/NADH Ratio
p=0.066
p=0.061
NADH
NAD+
NAD+/NADH
G
VO2
VO2/ BW (ml/min/kg)
VCO2 / VO2 Ratio
RQ
light
dark
Time after fasted (hr)
0-12
12-24
24-36
36-48
H
Fed
Fasted 48hr
Locomotor activity (count x 1000)
Light
Dark
I
Fed
Fasted 24hr
Body temperature (°C)
Time after 4°C (hr)
J
+/+
-/-
N.S.
*
Run time (min)
Fed
Fasted

2 mM at 40 min after the injection (data not shown). Under this condition, the rate of acetate oxidation measured was still significantly lower in *AceCS2*$^{-/-}$ mice (Figure 2C). Oxidation of ketone bodies was similar, irrespective of genotype (Figure 2D), indicating that ketone body utilization is normal in *AceCS2*$^{-/-}$ mice.

Together with our previous report showing that [$^{14}$C]acetate is incorporated into $CO_2$ in AceCS2-transfected cells (Fujino et al., 2001), these data indicate that, in mice, acetate oxidation to form $CO_2$ and ATP requires AceCS2. Previous studies showed that an appreciable amount of acetate is generated in liver by hepatic acetyl-CoA hydrolase, a ubiquitous peroxisome enzyme, and that this acetate can subsequently be utilized by extrahepatic tissues (Leighton et al., 1989; Murthy and Steiner, 1973; Seufert et al., 1974). We propose a model in which acetate is generated in liver from fatty acids and released into the circulation under conditions when glucose is low, such as 48 hr fasting or low-carbohydrate/ high-fat diet. AceCS2 is necessary for salvaging this acetate for use in extrahepatic tissues such as skeletal muscle and BAT, where acetate is reactivated for reentry to the mitochondrial TCA cycle to generate ATP and heat (Figure 2E).

### Adult *AceCS2*$^{-/-}$ Mice Exhibit Low Body Temperature and Reduced Capacity to Sustain Running Exercise under a Fasting Condition

To further evaluate the physiological role of acetate oxidation, 12-week-old *AceCS2*$^{-/-}$ mice were freely fed a standard rodent diet or fasted for 48 hr. During normal fed states, there was no significant difference in core temperature between *AceCS2*$^{+/+}$ and *AceCS2*$^{-/-}$ mice (Figure 3A). After 48 hr of fasting, *AceCS2*$^{+/+}$ mice were able to maintain their core body temperatures, but *AceCS2*$^{-/-}$ mice had significantly lower core body temperatures (Figure 3A). These data demonstrate that acetate activation by AceCS2 is important for maintenance of normal body temperature, likely as a result of heat production during fasting. Indeed, the mRNA levels in BAT of AceCS2 were 4-fold higher under the fasted condition than under the fed condition, suggesting that AceCS2 has an important role during fasting condition (Figure 3B).

In mice, BAT and skeletal muscle are the main thermogenic tissues in which oxidation of fatty acid, stimulated by the sympathetic nervous system, generates heat through uncoupling proteins (UCPs) present in mitochondria (Spiegelman and Flier, 2001). During fasting, the quantity and morphology of mitochondria in BAT and skeletal muscle are indistinguishable between *AceCS2*$^{+/+}$ mice and sex- and age-matched *AceCS2*$^{-/-}$ mice (Figure S2A). Oxidative proteins such as UCPs are thought to be important in thermogenesis (Matthias et al., 2000; Spiegelman and Flier, 2001). The mRNA levels of UCP1 in the BAT or UCP2 and UCP3 in the skeletal muscle did not differ significantly between *AceCS2*$^{+/+}$ and *AceCS2*$^{-/-}$ mice. Other thermogenic molecules PGC1$\alpha$ and PPAR$\delta$ also did not differ in mRNA levels (Figure S2B and data not shown).

To evaluate substrate supply, we determined the levels of various metabolites in the plasma of fed and 48 hr fasted 12-week-old male *AceCS2*$^{+/+}$ and *AceCS2*$^{-/-}$ mice (Table S2). There was no significant change in plasma glucose or in NEFA and ketone body levels between *AceCS2*$^{+/+}$ and *AceCS2*$^{-/-}$ mice (Table S2). There was also no significant difference in the percentage of fat mass between fed *AceCS2*$^{-/-}$ and *AceCS2*$^{+/+}$ mice as assessed by dual-energy X-ray absorption (DEXA) (Table S2). However, plasma acetate was 5- to 10-fold higher in *AceCS2*$^{-/-}$ mice as compared to *AceCS2*$^{+/+}$ mice under both fed and fasted conditions (Figure 3C). These data indicate that acetate utilization is impaired in *AceCS2*$^{-/-}$ mice, implying that a deficit in extrahepatic acetate utilization causes fasting-induced hypothermia. Acetyl-CoA levels were decreased by 75% in fasted *AceCS2*$^{-/-}$ mice (Figure 3D). NADH and ATP levels in skeletal muscles of fasted *AceCS2*$^{-/-}$ mice were significantly reduced compared to those found in *AceCS2*$^{+/+}$ mice (Figures 3E and 3F). These data indicate that AceCS2 plays a pivotal role in supplying acetyl-CoA for ATP production during 48 hr of fasting. Oxygen consumption was significantly increased after 36 hr fasting, and locomotor activity was not reduced (Figures 3G and 3H).

The hypothermia in *AceCS2*$^{-/-}$ mice also differs from adaptive hypothermia in response to cold (Lowell and Spiegelman, 2000). Exposure of these *AceCS2*$^{-/-}$ mice to low temperature (4°C) did

Figure 3. *AceCS2*-Deficient Mice Exhibit Low Body Temperature and Reduced Exercise Capacity during Fasting

(A) Core temperature of male mice (12 weeks old) fed on normal chow diet was monitored after 48 hr fasting (*AceCS2*$^{+/+}$, n = 8; *AceCS2*$^{-/-}$, n = 7). *$p < 0.05$ compared to *AceCS2*$^{+/+}$.

(B) Relative mRNA expression levels of AceCS2 in BAT of male mice (12 weeks old, six to seven per genotype). **$p < 0.01$ compared to *AceCS2*$^{+/+}$.

(C) Plasma acetate levels of male mice (12 weeks old) fed or fasted for 48 hr (fed *AceCS2*$^{+/+}$, n = 4; fasted *AceCS2*$^{+/+}$, n = 4; fed *AceCS2*$^{-/-}$, n = 4; fasted *AceCS2*$^{-/-}$, n = 4).

(D) Acetyl-CoA levels in gastrocnemius muscle from 48 hr fasted male *AceCS2*$^{+/+}$ and *AceCS2*$^{-/-}$ mice (12 weeks old) were measured (*AceCS2*$^{+/+}$, n = 7; *AceCS2*$^{-/-}$, n = 8).

(E) ATP content is markedly reduced in *AceCS2*$^{-/-}$ mice. ATP and AMP contents of gastrocnemius muscle from male *AceCS2*$^{+/+}$ and *AceCS2*$^{-/-}$ mice were measured at 12 weeks of age (*AceCS2*$^{+/+}$, n = 7; *AceCS2*$^{-/-}$, n = 8). **$p < 0.01$ compared to *AceCS2*$^{+/+}$.

(F) $NAD^+$ and NADH levels and $NAD^+$/NADH ratio in gastrocnemius muscle and BAT of 48 hr fasted male *AceCS2*$^{+/+}$ and *AceCS2*$^{-/-}$ mice (12 weeks old) (*AceCS2*$^{+/+}$, n = 4; *AceCS2*$^{-/-}$, n = 4).

(G) Oxygen consumption ($VO_2$) (left panel), average of $VO_2$ (center panel), and RQ (respiratory quotient) (right panel) were determined in fasted male mice (12 weeks old) by indirect calorimetry (*AceCS2*$^{+/+}$, n = 6; *AceCS2*$^{-/-}$, n = 5).

(H) Total locomotor activity of male mice (14 weeks old) was measured by beam breaks in the light and dark periods (*AceCS2*$^{+/+}$, n = 12; *AceCS2*$^{-/-}$, n = 12).

(I) Male mice (12 weeks old) given food and water ad libitum were subjected to cold (4°C) (left panel) (*AceCS2*$^{+/+}$, n = 10; *AceCS2*$^{-/-}$, n = 11). Male mice (12 weeks old) fasted for 24 hr and given water ad libitum were subjected to cold (4°C) (right panel) (*AceCS2*$^{+/+}$, n = 7; *AceCS2*$^{-/-}$, n = 8). Core temperature was monitored over a 5 hr period.

(J) Male mice (12 weeks old, nine per genotype) were subjected to a run-to-exhaustion protocol on a motorized treadmill under fed conditions and 48 hr fasted conditions (*AceCS2*$^{+/+}$, n = 9; *AceCS2*$^{-/-}$, n = 9). *$p < 0.05$ compared to fed.

All values are mean ± SEM.